

Revision 2

Cu diffusion in a basaltic melt

Peng Ni¹, Youxue Zhang

Department of Earth and Environmental Sciences, University of Michigan, Ann Arbor, MI 48109-1005, USA

ABSTRACT

Recent studies suggest a potential role of diffusive transport of metals (e.g. Cu, Au, PGE) in the formation of magmatic sulfide deposits and porphyry-type ore deposits. However, diffusivities of these metals are poorly determined in natural silicate melts. In this study, diffusivities of copper in an anhydrous basaltic melt (<10 ppm H₂O) were measured at temperatures from 1298 to 1581 °C, and pressures of 0.5 GPa, 1 GPa and 1.5 GPa. Copper diffusivities in anhydrous basaltic melt at 1 GPa can be described as:

$$D_{\text{Cu}}^{\text{basalt}} = \exp\left[-(14.12 \pm 0.50) - \frac{11813 \pm 838}{T}\right]$$

where $D_{\text{Cu}}^{\text{basalt}}$ is the diffusivity in m²/s, T is the temperature in K, and errors are given at 1 σ level.

A fitting of all experimental data considering the pressure effect is:

$$D_{\text{Cu}}^{\text{basalt}} = \exp\left[-(13.59 \pm 0.81) - \frac{(12153 \pm 1229) + (620 \pm 241)P}{T}\right]$$

where P is the pressure in GPa, which corresponds to a pre-exponential factor $D_0 = (1.25$

$\times 2.2) \times 10^{-6}$ m²/s, an activation energy $E_a = 101 \pm 10$ kJ/mol at $P = 0$, and an activation volume

$V_a = (5.2 \pm 2.0) \times 10^{-6}$ m³/mol.

¹Corresponding author. *E-mail address*: pengni@umich.edu

19 The diffusivity of copper in basaltic melt is high compared to most other cations, similar
20 to that of Na. The high copper diffusivity is consistent with the occurrence of copper mostly as
21 Cu^+ in silicate melts at or below NNO. Compared to the volatile species, copper diffusivity is
22 generally smaller than water diffusivity, but about 1 order of magnitude higher than sulfur and
23 chlorine diffusivities. Hence, Cu partitioning between a growing sulfide liquid drop and the
24 surrounding silicate melt is roughly in equilibrium, whereas that between a growing fluid bubble
25 and the surrounding melt can be out of equilibrium if the fluid is nearly pure H_2O fluid. Our
26 results are the first copper diffusion data in natural silicate melts, and can be applied to discuss
27 natural processes such as copper transport and kinetic partitioning behavior in ore formation, as
28 well as copper isotope fractionation caused by evaporation during tektite formation.

29 **Keywords:** Copper diffusivity, kinetics, kinetic fractionation, copper isotope fractionation

30

31

INTRODUCTION

32 As an important base metal widely used in construction and industry, enrichment of
33 copper from a crustal average of 27 ppm ([Rudnick and Gao 2014](#)) to a typical minable
34 concentration of a few thousand ppm has attracted much attention from economic geologists.
35 Magmatic sulfide deposits and porphyry copper deposits are two main types of deposits that
36 produce copper. In particular, porphyry-type deposits account for ~57% of world's total
37 discovered copper ([Singer 1995](#)).

38 As described by [Naldrett \(1989\)](#), magmatic sulfide ore deposits are typically related to a
39 mafic or ultramafic magma. Cooling of the magma leads to the saturation of sulfur, and results in
40 the nucleation and growth of sulfide liquid drops. Since sulfide drops have higher density than

41 the silicate melt, they will sink through the magma chamber, at the same time growing and
42 scavenging ore elements (e.g. Cu, Ni, Au, Pt) from the surrounding magma. Given enough time,
43 these sulfide drops will settle to the bottom of the magma chamber and form sulfide ore deposits
44 (Zhang 2015). The mechanism for porphyry-type ore deposits to enrich copper is similar, but
45 instead of a sulfide liquid phase settling down in the magma chamber for magmatic sulfide
46 deposits, a fluid phase is saturated inside the magma, and rises through the magma chamber,
47 scavenging and transporting ore metals (e.g. Cu, Au, Mo) to the top of the magma chamber. In
48 both types of ore deposits, enrichment of the metals into the sulfide phase or fluid phase is
49 controlled by at least two factors: (i) partitioning of the metal elements into the sulfide or fluid
50 phase, which may depend on the presence of other elements, such as chlorine in the fluid phase,
51 and (ii) diffusion of the metal elements through the silicate melt to the sulfide or fluid phase. For
52 magmatic sulfide deposits, Mungall (2002a) modeled the kinetic control of metal partitioning
53 assuming a sulfide drop is static inside the magma, and found that the enrichment factors of
54 metals can differ by as large as a factor of 5 depending on the diffusivity of each metal. Zhang
55 (2015) developed a quantitative model for magmatic sulfide deposits considering both sulfide
56 sinking and growth in silicate magma. Metal behavior was also modeled in Zhang (2015)
57 parametrically, concluding that as long as the metal diffusivity is larger than or similar to sulfur
58 diffusivity that controls sulfide drop growth, partition of the metal into the sulfide liquid phase is
59 close to equilibrium. Both Mungall (2002a) and Zhang (2015) used the empirical model by
60 Mungall (2002b) to estimate metal diffusivities. The model of Mungall (2002b) indicates that
61 copper diffusion is much faster than sulfur diffusion. Therefore, both authors concluded that
62 partition of copper into the sulfide phase is close to equilibrium. On the other hand, Huber et al.
63 (2012) developed a model for metal enrichment and transport by a fluid phase in a porphyry

64 system, and suggested that the efficiency of copper enrichment is dependent on the relative
65 diffusivity of copper to that of chlorine. [Huber et al. \(2012\)](#) used copper diffusion data from [von](#)
66 [der Gonna and Russel \(2000\)](#), with copper diffusivity being 1 order of magnitude smaller than
67 chlorine diffusivity. Therefore, copper partition into the fluid phase would not reach equilibrium
68 if the fluid bubbles ascend rapidly according to [Huber et al. \(2012\)](#).

69 In addition to metal enrichment processes discussed above, some other processes in ore
70 formation might also be kinetically controlled. For example, in magmatic sulfide deposits, after
71 sulfide liquid accumulation at the bottom of the magma chamber to form a sulfide liquid pool,
72 the interaction between the sulfide liquid pool and the magma might be diffusion-controlled
73 ([Mungall 2002a](#)). At the same time, metal extraction from other minerals into the sulfide melts is
74 controlled by diffusion of the metal in the mineral phase (e.g., extraction of Ni from olivine;
75 [Zhang 2015](#)). For porphyry-type ore deposits, re-dissolving of the sulfides and transport of their
76 metal elements from the more mafic magma to the silicic magma by a magmatic volatile phase is
77 also partially controlled by diffusivities of the metal elements in the melts ([Nadeau et al. 2010,](#)
78 [2013](#)).

79 Besides roles in copper ore formation, copper diffusivity is also an important parameter
80 in discussing copper isotope fractionation. [Moynier et al. \(2010\)](#) measured copper isotopes in
81 tektites, and found copper isotopes are more fractionated than zinc isotopes in the same set of
82 tektite samples. This is contrary to the notion that fractionation is due to volatile loss because
83 zinc has lower half-condensation temperature and is hence more easily lost than copper. The
84 authors explained their results by a higher diffusivity of copper than zinc in silicate melts,
85 implying that the isotope fractionation process was diffusion-limited.

86 Copper diffusion data in silicate melts are limited. Although there is a single study of
87 copper diffusivity in a $\text{Na}_2\text{Si}_2\text{O}_5$ melt by [von der Gonna and Russel \(2000\)](#), there are currently no
88 copper diffusion data in natural silicate melts. Cu diffusivity in the $\text{Na}_2\text{Si}_2\text{O}_5$ melt is unlikely
89 applicable to Cu diffusion during copper ore formation from a natural silicate melt. Even though
90 there is an empirical model by [Mungall \(2002b\)](#) to estimate diffusivity, as [Behrens and Hahn](#)
91 [\(2009\)](#) and [Zhang et al. \(2010\)](#) pointed out, [Mungall \(2002b\)](#)'s diffusivity model may be orders
92 of magnitude off in predicting diffusivities. Hence, experimental data are necessary for more
93 quantitative prediction of the diffusion effects.

94 In this study, diffusion couple experiments are carried out to obtain copper diffusivities in
95 a basaltic melt, and the results are used to discuss copper enrichment in ore formation, and to
96 speculate on kinetic controls of copper isotope fractionation.

97

98 **EXPERIMENTAL AND ANALYTICAL METHODS**

99 **Starting glasses**

100 Two glasses with the same major element composition but different copper
101 concentrations were synthesized for the diffusion couple experiments. A major element
102 composition of Etna basalt was chosen since it has been well studied in terms of melt properties:
103 both melt viscosity and sulfur diffusivity have been measured for this melt composition
104 ([Giordano and Dingwell 2003](#); [Freda et al. 2005](#)).

105 In order to synthesize the starting glasses, a total weight of ~6.5 g of oxides (SiO_2 , TiO_2 ,
106 Al_2O_3 , Fe_2O_3 , MgO) and carbonates (CaCO_3 , Na_2CO_3 , K_2CO_3) were weighed based on the target
107 composition of Etna basalt ([Freda et al. 2005](#)) and well mixed under alcohol in an agate mortar.

108 Then the mixture of the oxides and carbonates was divided into two halves, one of which was
109 doped with Cu_2O to contain ~ 1200 ppm Cu. Afterwards, approximately 0.6 g of the copper-free
110 mixture and copper-containing mixture were put into separate graphite crucibles and fused at
111 1300°C for 3 hours together inside a Deltech furnace under a constant N_2 flow. After fusing, the
112 two crucibles were taken out of the furnace and cooled in air to form two glass beads with a
113 diameter of ~ 8 mm.

114 The glasses synthesized were examined under optical microscope to ensure that they are
115 bubble free, crystal free and homogeneous in color. A center section was cut from each glass
116 bead and analyzed by electron microprobe to check its homogeneity before it was used for
117 diffusion couple experiments. Average compositions of the synthesized glasses are shown in
118 Table 1. In general, microprobe data show that the composition of the synthesized glass matches
119 the target composition fairly well (difference < 1 wt% for each major component). FeO
120 concentration was found to decrease slightly ($\sim 8\%$ relative) towards the surface of the glass
121 beads. Cu concentration was also found to be slightly inhomogeneous, with lower concentration
122 near the surface of the glass beads (~ 1000 ppm) than at the center of the glass beads (~ 1300 ppm)
123 (Fig. 1). To avoid possible effects of inhomogeneity in glass composition to our experiments,
124 only center parts of the synthetic glasses were used for diffusion couple experiments.

125 H_2O and CO_2 concentrations in the synthetic Etna basaltic glasses are below ~ 10 ppm
126 and ~ 100 ppm, respectively, based on FTIR measurements using a Perkin-Elmer Spectrum GX
127 FTIR spectrometer at the University of Michigan.

128

129 **Experimental procedure**

130 All diffusion couple experiments were conducted in a piston-cylinder apparatus at the
131 University of Michigan. An illustration of the experimental design for our diffusion couple
132 experiments can be found in Fig. 2, and the experimental procedures are as follows. First, two
133 glass cylinders with a diameter of 2.0 mm and height of 1.5 mm were prepared, one from copper-
134 free and the other from copper-containing synthetic glass beads. The choice of 1.5 mm height of
135 each glass cylinder used in our experiments is a compromise between two factors. One factor is
136 that shorter cylinders lead to shorter experimental charge and hence smaller temperature
137 variation across the whole charge. The other is that the cylinder must be tall enough so that Cu
138 diffusion would not reach the boundary of the glass during the experiment. The glass cylinders
139 were doubly polished using progressively finer silicon carbide sandpapers and a finish on 0.1- μm
140 alumina powder. Afterwards, the two glass cylinders were ultrasonically cleaned in acetone and
141 then in alcohol. After drying in vacuum for about 1 hour, the two glass cylinders were placed
142 together and fit snugly into a 4.0-mm outer-diameter graphite capsule. The copper-free glass was
143 placed on top since it is expected to have a slightly lower density. The graphite capsule was fit
144 into an MgO pressure medium, then placed inside a graphite furnace, and then into a BaCO₃
145 outer pressure medium. Geometry of the sample assemblage was designed so that the interface is
146 at the center of the graphite furnace to minimize temperature gradient across the capsule (Fig. 2).
147 A type-S thermocouple (Pt90Rh10-Pt) was used to measure the temperature during an
148 experiment. The length of each part of the sample assemblage was measured after an experiment
149 to examine whether the interface was at the center of the graphite furnace during the experiment.
150 The distance of the thermocouple tip to the diffusion interface was typically 2.5 to 3 mm.
151 Temperature correction was made using the calibration of [Hui et al. \(2008\)](#). Temperature at the

152 interface of the diffusion couple was used as the experimental temperature. The temperature at
153 the two ends of the diffusion couple is estimated to be 10 to 20 °C below the interface
154 temperature using the calibration of [Hui et al. \(2008\)](#).

155 Experiments were conducted at pressures of 0.5 to 1.5 GPa at a 0.5 GPa increment. A 5%
156 pressure correction is applied based on calibration by [Ni and Zhang \(2008\)](#) on the same piston
157 cylinder apparatus. During an experimental run, the pressure was first increased slowly and
158 smoothly to 15% higher than the target pressure (10% in the case of 1.5 GPa experiment) using a
159 pressure controller. Then the whole sample assemblage was relaxed at this pressure and 200 °C
160 for at least 2.5 hours to close gaps inside the assemblage. Both pressure and temperature were
161 maintained automatically in this step. After relaxation, the temperature was brought up to the
162 designated temperature in ~60 s by a programmed heating procedure. No temperature overshoot
163 occurred during heating-up, and temperature fluctuation was within ± 1 °C during the
164 experiments. Due to high Cu diffusivity, only a short duration was needed in the diffusion couple
165 experiments (2 to 7 minutes at 1298 °C to 1581 °C) to generate a long enough profile. After a
166 designated duration, the assemblage was quenched with a cooling rate of about 100 °C/s (based
167 on direct measurement) by turning off the power. During quench, the pressure was maintained by
168 a manually controlled ENERPAC electric pump (except for Cudiffcp 4.4 and Cudiffcp 7.2, for
169 which the pressure was maintained by the pressure controller). The whole sample assemblage
170 was then preserved inside an epoxy resin disc and polished to expose the center section for
171 electron microprobe analysis.

172 Since the experimental duration was only 2 to 7 minutes, the effect of heating up (taking
173 ~1 min) needs to be considered. Quenching is rapid and hence the effect is small, but the small
174 effect is also accounted for in the following correction applied to obtain the effective duration for

175 all experiments. Based on the solution to the diffusion problem for time-dependent D (e.g.,
176 [Zhang, 2008, Eq. 3-54b](#)), the following equation was used to calculate the effective duration at
177 the experimental temperature T_0 :

$$178 \quad t_c = \frac{\int_0^t \exp(-E / RT) dt}{\exp(-E / RT_0)} \quad (2)$$

179 where t_c is the effective duration, E is the activation energy for Cu diffusion, R is the gas
180 constant, T is recorded experiment temperature (including temperature recorded during heating
181 up and that during cooling down) corrected to the interface position, and T_0 is the plateau
182 interface temperature. At the beginning an estimated E was used for the effective duration
183 correction. After enough experiments were done, E was obtained by fitting the Arrhenius
184 equation and t_c was corrected again until t_c and E do not change anymore. Copper diffusion has a
185 small activation energy, leading to a relatively large duration correction of ~35 s.

186

187 **Analytical methods**

188 Major element composition and copper concentration profiles were measured in WDS
189 mode using the Cameca SX-100 electron microprobe at the University of Michigan. Major oxide
190 concentrations (SiO_2 , TiO_2 , Al_2O_3 , FeO_t , MgO , CaO , Na_2O and K_2O) of the synthetic glasses
191 were measured with an acceleration voltage of 15 kV, a beam current of 10 nA in focused mode,
192 and a counting time of 30 to 40 seconds on the peak and 15 to 20 seconds on each side of the
193 backgrounds. The following standards were used for the microprobe analysis: albite (ALBA) for
194 Na, forsterite (FOBO) for Mg and Si, sillimanite (SILL) for Al, potassium feldspar (GKFS) for K,
195 wollastonite (WOLL) for Ca, geikielite (GEIK) for Ti, and ferrosilite (FESI) for Fe. Cu
196 concentrations were measured in separate sessions using a point beam with an acceleration

197 voltage of 15 kV and a beam current of 40 nA. The standard for Cu concentration measurement
198 is chalcopyrite (CPY). Three spectrometers were employed to count Cu at the same time. The
199 counting time is 240 s on the Cu $K\alpha$ peak and 120 s on either side of the background to achieve a
200 detection limit of ~ 80 ppm for Cu. The analytical error given by the microprobe based on
201 counting statistics is ~ 80 ppm (1σ). NIST SRM 610 was used as a secondary standard for Cu in
202 our analysis. The average concentration of Cu in SRM 610 was reported by [Pearce et al. \(1997\)](#)
203 to be 422 ± 42 ppm. Our microprobe analysis yielded a Cu concentration of 464 ppm to 516 ppm
204 on SRM 610. The shift of absolute concentrations results in a shift of the entire copper diffusion
205 profile. However, if the amount of shift were similar for both the low and high copper
206 concentration ends, the diffusivity obtained from the profile would not be affected. In order to
207 evaluate whether the shift in absolute copper concentration has significant effect on copper
208 diffusivity, the sample Cudiffcp 3.1 was analyzed twice on two different days. The entire copper
209 concentration profile measured on two days shifted ~ 200 ppm from each other. However, after
210 the background correction, the two profiles measured on different days closely match each other
211 (Fig. 3). The diffusivities fitted from the two analyses of different days are $<2\%$ different from
212 each other, which is much smaller than the fitting error (1σ fitting error is about 10%) and hence
213 negligible.

214

215

RESULTS

Copper diffusion profiles and fitting

216
217 Ten successful diffusion couple experiments have been conducted. In addition to the 10
218 experiments reported here in Table 1, two more experiments were carried out but are classified
219 as unsuccessful. One experiment at 0.5 GPa and 1300 °C shows abnormal concentration profile,

220 which might be due to initial Cu concentration inhomogeneity. The other experiment at 1.5 GPa
221 and 1300 °C crystallized because the pressure was too high for the given temperature. Both
222 experiments are excluded from the data.

223 Fig. 4 shows optical microscope images of two successful experiments. For each
224 diffusion couple, at least three Cu concentration traverses ~250 μm apart from each other were
225 measured to examine the reproducibility and possible convection. In five out of the ten
226 experiments (Cudiffcp 1.2, Cudiffcp 3.1, Cudiffcp 4.2, Cudiffcp 4.3 and Cudiffcp 4.4), the
227 interface survived the quench process and the sample glasses were crack-free after the
228 experiment. In these cases, the physical interface position was indicated by the two dents on both
229 sides of the glasses, as shown in Fig. 4a.

230 For the other five experiments (Cudiffcp 1.1, Cudiffcp 2.1, Cudiffcp 5.1, Cudiffcp 6.1
231 and Cudiffcp 7.2), a crack occurred almost exactly along the interface (Fig. 4b). In order to
232 prevent loss of glass during polish, epoxy was added multiple times to protect the cracks. After
233 microprobe analyses, copper concentration profiles on both sides of the crack were compared: if
234 necessary, a distance correction is made so that the profile across the crack is smooth. As a result,
235 a 7.5 μm and 12.5 μm correction to the concentration profiles was applied for experiments
236 Cudiffcp 2.1 and Cudiffcp 6.1, while no correction was applied to experiments Cudiffcp 1.1,
237 Cudiffcp 5.1 and Cudiffcp 7.2.

238 Cu concentration profiles in all experiments besides Cudiffcp 3.1 are shown in Fig. 5.
239 The concentration profiles were fit by the solution to a one-dimensional diffusion couple with
240 constant diffusivity (Crank 1975):

$$241 \quad C = \frac{C_0 + C_1}{2} + \frac{C_0 - C_1}{2} \operatorname{erf} \frac{x - x_0}{\sqrt{4Dt}} \quad (3)$$

242 where C_0 is the initial Cu concentration at the Cu-free half of the diffusion couple (defined as $x -$
243 $x_0 > 0$); C_1 is the initial Cu concentration at the Cu-bearing half (defined as $x - x_0 < 0$); D is copper
244 diffusivity and x_0 is the position of the interface. Since copper diffusivity is high, there is concern
245 that copper diffusion might have reached the ends of the diffusion couple. This would cause error
246 in fitting using Eq. 3, which assumes an infinite diffusion medium. Visual examination of the
247 data and fitting of the profiles indicate that for the longer-duration or higher-temperature
248 experiments (Cudiffcp 1.1, Cudiffcp 5.1 and Cudiffcp 7.2) diffusion seems to have reached the
249 two ends. Numerical fitting using the solution for finite diffusion medium was carried out for
250 these three experiments (curves shown in Fig. 5), and the resulting diffusivities were only 3-5%
251 higher than that assuming infinite diffusion medium.

252

253 **Temperature and pressure dependence of copper diffusivity**

254 Experimental run conditions and results for all successful experiments are summarized in
255 Table 2. An Arrhenius plot of all copper diffusivities obtained in this study is shown in Fig. 6.
256 Diffusion data of the five experiments at 1 GPa and 1314-1575 °C in anhydrous basaltic melt can
257 be expressed by the following Arrhenius relation:

$$258 \quad D_{\text{Cu}}^{\text{basalt}} = \exp\left[-(14.12 \pm 0.50) - \frac{11813 \pm 838}{T}\right], \quad r^2=0.985 \quad (4)$$

259 where $D_{\text{Cu}}^{\text{basalt}}$ is in m^2/s , T is temperature in K, and errors are at 1σ level. The above equation
260 reproduces the five experimental $\ln D$ values to within 0.09 $\ln D$ units. The activation energy
261 corresponding to Eq. 4 is 98.2 ± 7.0 kJ/mol. This small activation energy (~ 100 kJ/mol) means
262 that the temperature dependence of copper diffusivity is relatively small compared to other
263 elements, and is consistent with Cu diffusing as Cu^+ .

264 To evaluate the pressure effect on copper diffusivity, two experiments were done at 1.5
265 GPa and three experiments were done at 0.5 GPa (see Fig. 6). Two of the three 0.5 GPa
266 experiments gave diffusivities that are ~20% higher than the 1 GPa diffusivities, while
267 diffusivity from the other 0.5 GPa experiment fell 12% below the 1 GPa trend. Two 1.5 GPa
268 experiments gave diffusivities 12% and 29% below the 1 GPa diffusivities respectively.
269 Although the 0.5 GPa experiments have relatively larger errors (these are still small errors for
270 diffusion studies), a fit of all measured copper diffusivities at 1298 °C to 1581 °C and 0.5 to 1.5
271 GPa gives:

$$272 \quad D_{\text{Cu}}^{\text{basalt}} = \exp \left[-(13.59 \pm 0.81) - \frac{(12153 \pm 1229) + (620 \pm 241)P}{T} \right], r^2 = 0.938 \quad (5)$$

273 where $D_{\text{Cu}}^{\text{basalt}}$ is diffusivity in m^2/s , T is temperature in K, P is pressure in GPa, and errors are at
274 1σ level. Eq. 5 corresponds to a pre-exponential factor $D_0 = (1.25 \times 2.2) \times 10^{-6} \text{ m}^2/\text{s}$, an activation
275 energy $E_a = 101 \pm 10 \text{ kJ/mol}$ and an activation volume $V_a = (5.2 \pm 2.0) \times 10^{-6} \text{ m}^3/\text{mol}$ for copper
276 diffusion in anhydrous basaltic melt. The above equation is able to reproduce all our
277 experimental $\ln D$ values to within 0.23 $\ln D$ units.

278

279 **Possible complications and other sources of error**

280 Since basaltic melts have low viscosities at our experimental condition (about 10^0 to $10^{1.3}$
281 $\text{Pa}\cdot\text{s}$ at temperatures from 1581 °C to 1298 °C using the viscosity model for Etna basalt by
282 [Giordano and Dingwell 2003](#)), there is concern about whether convection has occurred during
283 the experiments. Effort was made to examine whether convection is an issue in our experiments.
284 First, at least three traverses 200 μm to 300 μm apart from each other were measured on every
285 sample. If convection occurred, the three traverses would likely diverge, and diffusivities

286 obtained from these traverses may be significantly different from each other. The results show
287 that, diffusivities fitted to individual traverses in one sample are typically within ~20% from the
288 overall diffusivity, indicating no obvious convection. Second, two experiments (Cudiffcp 1.1 and
289 Cudiffcp 1.2) were conducted at the same temperature and pressure but with different duration
290 (465 s vs 163 s, almost a factor of 3 difference). As can be found in Table 2, relative diffusivity
291 difference between the two experiments is only about 8%, within our experimental error. Both
292 the consistency between diffusivities from Cudiffcp 1.1 and Cudiffcp 1.2 and the agreement
293 between different traverses in the same experiment suggest that the occurrence of convection is
294 unlikely in our experiments.

295 Temperature uncertainty may cause error in the data. As discussed in Methods,
296 temperature at the two ends of the diffusion couple can be 10 to 20 °C lower than the interface
297 temperature. Hence, the error caused by temperature uncertainty is estimated using this
298 maximum temperature uncertainty of 20 °C. Based on the activation energy of 98.2 kJ/mol for
299 Cu diffusivity at 1 GPa, the uncertainty of 20 °C can result in errors in D_{Cu} of 10% at 1300 °C
300 and 7% at 1600 °C. The uncertainty in Cu diffusivity due to pressure uncertainty is negligible
301 because copper diffusivity changes less than 20% when pressure changes by 0.5 GPa.

302 Another possible source of error is the effective run duration contributed by heating and
303 cooling. As a compromise to the high Cu diffusivity, most of our experiments were designed to
304 be only ~2 min long. Under this circumstance, the heating and quenching processes contribute
305 about 20% to 30% to the effective run duration, meaning Cu diffusivity is changed by 20% to
306 30% with the duration correction. However, the method we used to correct the duration (Eq. 2) is
307 accurate if the activation energy of Cu diffusion is constant.

308 As mentioned earlier, cracks occurred along the interface of five samples during quench
309 (Cudiffcp 1.1, Cudiffcp 2.1, Cudiffcp 5.1, Cudiffcp 6.1 and Cudiffcp 7.2) and the cracks are
310 almost perfectly horizontal, and hence the distance across the crack cannot be determined by
311 comparing different traverses. For these five experiments, corrections were done by comparing
312 the trend of copper concentration profiles on both sides of the crack. As a result, a 7.5 μm and
313 12.5 μm correction to the concentration profiles was applied for experiments Cudiffcp 2.1 and
314 Cudiffcp 6.1, while no correction was applied to experiment Cudiffcp 1.1, Cudiffcp 5.1 and
315 Cudiffcp 7.2. This resulted in a 3% increase in diffusivity obtained from Cudiffcp 2.1 and a 2%
316 increase in diffusivity obtained from Cudiffcp 6.1.

317 The synthetic starting glasses are not perfectly homogeneous in copper concentration. In
318 the 8-mm-diameter copper-bearing synthetic glass, copper concentration can be ~ 1300 ppm at
319 the center and ~ 1000 ppm near the boundary (Fig. 1). However, considering that the glass
320 cylinder used for experiments is only about 1.5-mm tall, the copper concentration difference
321 across the glass cylinder is ~ 100 ppm, which is only slightly above our analytical error of ~ 80
322 ppm. Therefore the Cu concentration gradient in the starting glasses is unlikely to cause
323 significant error.

324

325

DISCUSSION

326 **Comparison with existing copper diffusivity data**

327 For multivalent ions, valence state of the ion plays an important role in its diffusivity in
328 silicate melts and minerals. Ions in the lower valence state typically have higher diffusivities
329 because of the weaker bonding between these ions and surrounding melt structure (Zhang 2010).
330 Examples of multivalent ions in silicate melts include Fe^{2+} and Fe^{3+} , Sn^{2+} and Sn^{4+} , etc. Copper

331 is also a multivalent element in the natural system, and is commonly found as 0, +1 or +2 in
332 natural occurrence. In the study of copper solubility in a mafic melt, [Ripley and Brophy \(1995\)](#)
333 plotted log copper solubility versus $\log f_{O_2}$, and found that copper dissolves into the melt
334 predominantly in +1 valence state at or below NNO. The high Cu diffusivity and low activation
335 energy for Cu diffusion observed in our study are consistent with Cu being univalent. Therefore
336 in this study, we regard our measured copper diffusivity as Cu^+ diffusivity.

337 As mentioned in the Introduction, we know of only one study reporting Cu^+ diffusivities
338 in $\text{Na}_2\text{Si}_2\text{O}_5$ melt ([von der Gonna and Russel 2000](#)) using a voltammetry method. They reported
339 Cu^+ diffusivity to be $5.01 \times 10^{-11} \text{ m}^2/\text{s}$ at 1100 °C with activation energy of 92.1 kJ/mol. Their
340 diffusivities of copper in $\text{Na}_2\text{Si}_2\text{O}_5$ glass melt are plotted in Fig. 7 (green open squares) to
341 compare with those measured in this study (red solid circles, diamonds and triangles). Cu^+
342 diffusivities in $\text{Na}_2\text{Si}_2\text{O}_5$ glass melt are smaller than those in basaltic melt by a factor of about 3
343 with similar activation energy.

344 [Mungall \(2002b\)](#) developed a model to calculate ion diffusivities in silicate melt.
345 Calculated Cu^+ diffusivities in basaltic melt using his model are plotted in Fig. 7 as a grey solid
346 line, and are about 3 to 5 times the diffusivities determined by our experiments. The model by
347 [Mungall \(2002b\)](#) shows larger errors in reproducing the diffusivities in the $\text{Na}_2\text{Si}_2\text{O}_5$ melt. At
348 1100°C, calculated Cu^+ diffusivities using his model are two orders of magnitude larger than the
349 experimental data by [von der Gonna and Russel \(2000\)](#).

350

351 **Comparison of copper diffusivity with that of other elements in anhydrous basaltic melts**

352 Diffusivity data for selected elements in basaltic melts are also plotted in Fig. 7. From the
353 figure, Cu diffusivity is almost identical to Na diffusivity at ~1400 °C, lower than Li diffusivity

354 by a factor of about 3 and significantly higher than diffusivities of all other cations shown in Fig.
355 7. At 1300 °C, Cu diffusivity is ~10 times Ca and Co diffusivity, 18 times Mg diffusivity, and
356 ~30 times S and Fe diffusivity. Since Cu diffusion has smaller activation energy than all other
357 elements shown in Fig. 7, when temperature increases, Cu diffusivity increases slower than other
358 elements. At 1500 °C Cu diffusivity is only ~5 to 10 times higher than Mg, Fe, Co, S and Ca.
359 However when temperature decreases, Cu diffusivity decreases slower than all other elements
360 shown in Fig. 7, and becomes larger than Na diffusivity. At 1100 °C, Cu diffusivity will be ~200
361 times Fe diffusivity, 67 times Mg diffusivity, 35 times Co diffusivity, ~25 times Ca diffusivity
362 and 2.5 times Na diffusivity.

363 To examine the role of valence and size of cations, the radius of Cu^+ was compared to
364 other monovalent cations. For self-consistency, the ionic radii of Li^+ , Cu^+ and Na^+ in octahedral
365 sites (0.076, 0.077, and 0.102 nm, respectively, [Shannon 1976](#)) are compared. If diffusivities of
366 univalent cations in a given melt are mainly determined by the ionic radii ([Mungall 2002b](#)), Cu^+
367 diffusivity would be similar to Li^+ diffusivity. The fact that Cu^+ diffusivity is a factor of 3
368 smaller than Li^+ diffusivity but similar to Na^+ diffusivity indicates that other ionic characters
369 (e.g., electronegativity, the presence of d electrons, different co-ordination number, etc.) also
370 play a role in determining the diffusion rate.

371

372 **Applications**

373 The role of copper diffusion in magmatic sulfide deposit formation has been discussed
374 above in the Introduction. The major conclusions by [Mungall \(2002a\)](#) and [Zhang \(2015\)](#) were
375 consistent in that, if the diffusivity of a metal is much larger than sulfur diffusivity in basaltic
376 melt, the partitioning of the metal into the sulfide phase can be regarded as in equilibrium. Both

377 [Mungall \(2002a\)](#) and [Zhang \(2015\)](#) used the diffusivity model by [Mungall \(2002b\)](#) to estimate
378 metal diffusivities in their study, and found Cu^+ to be one of the most mobile elements in basaltic
379 melt. Our results suggest that Mungall's model overestimated copper diffusivity in basaltic melt
380 by a factor of 2 to 4. However, our measured copper diffusivity is still ~ 30 times higher than
381 sulfur diffusivity in basaltic melt. Therefore copper partition into the sulfide melt can be
382 regarded as equilibrium partitioning in most cases.

383 High copper diffusivity in basaltic melt might also play a role in metal transport by a
384 magmatic vapor phase (MVP). [Nadeau et al. \(2013\)](#) carried out a melt-inclusion study on
385 samples from Merapi volcano, Indonesia, and found that copper was more enriched in shallower
386 felsic melts (~ 45 ppm) than in deeper mafic melts (~ 25 ppm), which is opposite to the trend
387 normally observed in arc magmas. The unusual behavior of Cu could not be explained by crystal
388 fractionation or combined assimilation and fractionation. [Nadeau et al. \(2010\)](#) suggested a
389 mechanism in which copper was transported from the mafic magma to the felsic magma by an
390 MVP enriched in copper. Since water diffusivity in basalt is high (Fig. 7), the growth of an MVP
391 inside the magma is rapid. In this process, because the diffusivity of copper is lower than that of
392 H_2O but higher than that of other metal elements (except for Li and Na), copper would not reach
393 equilibrium concentration in the MVP but would be more efficiently enriched in the aqueous
394 volatile phase than the other metal elements. One complication is that, the partition coefficient of
395 copper between the volatile phase and the silicate melt phase strongly depends on chlorine and
396 sulfur contents in the volatile phase (e.g., [Candela and Holland 1984](#); [Williams et al. 1995](#); [Simon](#)
397 [et al. 2006](#) and [Zajacz et al. 2008](#)). Hence, enrichment of copper in the MVP would be controlled
398 by diffusion of sulfur or chlorine from the silicate melt to the MVP. As can be seen in Fig. 7,
399 $D_{\text{Cu}} > D_{\text{Cl}} > D_{\text{S}}$ assuming water content in silicate melt does not change the sequence. Therefore,

400 in pure H₂O fluid phase, Cu concentration in the fluid phase would be even lower than that
401 indicated by the low partition coefficient, but if the fluid bubble is enriched in chlorine or sulfide,
402 copper partitioning between the fluid and melt phases would be roughly in equilibrium, while Cl
403 and S concentrations in the fluid bubble would be lower than that indicated by equilibrium
404 partitioning. [Nadeau et al. \(2013\)](#) did not specify the composition of the MVP in his study, but a
405 study by [Zajacz and Halter \(2009\)](#) found evidence for sulfur-rich vapor in melt and vapor
406 inclusions hosted by plagioclase. In that case, copper partitioning during the metal transportation
407 by an MVP is likely equilibrium partitioning again.

408 High copper diffusivity may also be responsible for rapid Cu loss from tektites, resulting
409 in large kinetic copper isotope fractionation. [Moynier et al. \(2010\)](#) measured copper isotope
410 ratios in tektites, and found almost all the tektites are greatly enriched in heavy Cu isotope ($+1.99\text{‰}$
411 $< \delta^{65}\text{Cu} < +6.98\text{‰}$), where $\delta^{65}\text{Cu} = ((^{65}\text{Cu}/^{63}\text{Cu})_{\text{sample}} / (^{65}\text{Cu}/^{63}\text{Cu})_{\text{standard}} - 1) \times 1000\text{‰}$. Because
412 tektites might have been heated to a temperature as high as $>2800\text{ °C}$ ([Walter 1967](#)) for a short
413 period of time, and the half-condensation temperature for copper is 1037 K ([Lodders 2003](#)),
414 [Moynier et al. \(2010\)](#) proposed that copper isotopes were fractionated by evaporation loss, with
415 lighter isotopes escaping more rapidly into the volatile phase. However, by comparing with their
416 previous study of zinc isotope fractionation in tektites ([Moynier et al. 2009](#)), the authors found
417 zinc isotopes to be less fractionated than copper isotopes in the same set of samples ($\delta^{66/64}\text{Zn}$ up
418 to 2.49‰ comparing to $\delta^{65/63}\text{Cu}$ up to 6.98‰). If Cu and Zn loss is due to open system
419 volatilization (such as Rayleigh fractionation in which a tektite droplet is uniform compositionally
420 and isotopically), because zinc has a much lower half-condensation temperature ($T_c \sim 726\text{ K}$,
421 [Lodders 2003](#)) than Cu, zinc isotopes would be more fractionated than copper isotopes, opposite
422 to the observations. [Moynier et al. \(2010\)](#) explained the more fractionated copper isotopes than

423 zinc isotopes by the higher diffusivity of Cu^+ than Zn^{2+} in silicate melts, and argued that the
424 isotopic fractionation in tektites was controlled by the competition between the evaporation flux
425 and the diffusion flux. They employed the diffusivity model by [Mungall \(2002b\)](#) and found Cu^+
426 diffusivity to be about 2 orders of magnitude higher than Zn^{2+} diffusivity, and used this result to
427 explain why copper isotopes are more fractionated than zinc isotopes. Using literature Zn^{2+}
428 diffusion data in rhyolitic melt ([Baker and Watson, 1988](#)) and our Cu^+ diffusion data, and
429 assuming melt composition does not affect Cu^+ diffusivity significantly (our preliminary data
430 reported in [Ni et al., 2015](#) show that Cu^+ diffusivity in anhydrous rhyolitic melt is only ~50%
431 smaller than Cu^+ diffusivity in basalt), Cu^+ diffusivity is about 3 orders of magnitude higher than
432 Zn^{2+} diffusivity (Fig. 7). Hence, Cu and Zn diffusion data are consistent with the explanation by
433 [Moynier et al. \(2010\)](#).

434

435

IMPLICATIONS

436 Our copper diffusion data in basaltic melt show that, copper diffusivity in anhydrous
437 basaltic melt is as high as that of sodium at ~1400 °C, and has a small activation energy (~100
438 kJ/mol). The measured copper diffusivities are ~3 times smaller than the values predicted by a
439 previous diffusivity model in the same melt, and ~3 times larger than reported copper
440 diffusivities in the $\text{Na}_2\text{Si}_2\text{O}_5$ melt. In basaltic melt, copper diffusivity is ~30 times higher than
441 sulfur diffusivity, indicating that during the formation of magmatic sulfide deposit, when
442 immiscible sulfide liquid drops separate from the host magma and settle to the bottom of the
443 magma chamber, the partitioning of copper into the sulfide liquid phase can be regarded as
444 equilibrium partitioning. In the process of porphyry-type deposit formation, where metal
445 transport from the more mafic magma to the more felsic magma by a magmatic volatile phase is

446 possible, high diffusivity of copper also ensures the efficiency of copper diffusion into and away
447 from the volatile phase. Because of the high diffusivity of copper in basaltic melt, kinetic
448 limitation of copper partitioning during ore formation is less likely a concern. This also means
449 copper may be diffusively fractionated from other ore elements with smaller diffusivity.

450 The results of our study can also be used to discuss the kinetic role in evaporation loss
451 and isotope fractionation of volatile elements in impact glasses. The more fractionated copper
452 isotopes than zinc isotopes as observed in tektites can be explained by the higher diffusivity of
453 Cu^+ than Zn^{2+} in silicate melts, despite the lower condensation temperature for zinc than copper.
454 Similar processes may also happen to lunar volcanic and impact glasses on the surface of Moon.

455

456

ACKNOWLEDGEMENTS

457 We thank two anonymous reviewers for their constructive comments, and James Jolles
458 for informal comments. P. Ni thanks Zhengjiu Xu for training and help with piston-cylinder
459 experiments, Gordon Moore, Yang Chen and Yi Yu for help with microprobe analysis and
460 Chenghuan Guo for discussion about synthesizing glasses. This work was partially supported by
461 NSF grants EAR-1019440 and EAR-1524473. The electron microprobe used in this study was
462 acquired using NSF grant EAR-9911352.

463

464

REFERENCES CITED

465 Alletti, M., Baker, D.R., and Freda, C. (2007) Halogen diffusion in a basaltic melt. *Geochimica*
466 *et Cosmochimica Acta*, 71, 3570-3580.
467 Baker, D.R., and Watson, E.B. (1988). Diffusion of major and trace elements in compositionally
468 complex Cl- and F-bearing silicate melts. *Journal of Non-Crystalline Solids*, 102, 62-70.

- 469 Behrens, H., and Hahn, M. (2009) Trace element diffusion and viscous flow in potassium-rich
470 trachytic and phonolitic melts. *Chemical Geology*, 259, 63-77.
- 471 Candela, P.A., and Holland, H.D. (1984) The partitioning of copper and molybdenum between
472 silicate melts and aqueous fluids. *Geochimica et Cosmochimica Acta*, 48, 373-380.
- 473 Crank, J. (1975) *The Mathematics of Diffusion*. Oxford, UK: Clarendon Press.
- 474 Freda, C., Baker, D.R., and Scarlato, P. (2005) Sulfur diffusion in basaltic melts. *Geochimica et*
475 *cosmochimica acta*, 69, 5061-5069.
- 476 Giordano, D., and Dingwell, D. (2003) Viscosity of hydrous Etna basalt: implications for
477 Plinian-style basaltic eruptions. *Bulletin of Volcanology*, 65, 8-14.
- 478 Huber, C., Bachmann, O., Vigneresse, J.L., Dufek, J., and Parmigiani, A. (2012) A physical
479 model for metal extraction and transport in shallow magmatic systems. *Geochemistry,*
480 *Geophysics, Geosystems*, 13.
- 481 Hui, H., Zhang, Y., Xu, Z., and Behrens, H. (2008) Pressure dependence of the speciation of
482 dissolved water in rhyolitic melts. *Geochimica et Cosmochimica Acta*, 72, 3229-3240.
- 483 Lodders, K. (2003) Solar system abundances and condensation temperatures of the
484 elements. *The Astrophysical Journal*, 591, 1220.
- 485 Lowry, R.K., Reed, S.J.B., Nolan, J., Henderson, P., and Long, J.V.P. (1981) Lithium tracer-
486 diffusion in an alkali-basaltic melt—an ion-microprobe determination. *Earth and Planetary*
487 *Science Letters*, 53, 36-40.
- 488 Lowry, R.K., Henderson, P., and Nolan, J. (1982) Tracer diffusion of some alkali, alkaline-earth
489 and transition element ions in a basaltic and an andesitic melt, and the implications
490 concerning melt structure. *Contributions to Mineralogy and Petrology*, 80, 254-261.

- 491 Moynier, F., Beck, P., Jourdan, F., Yin, Q.Z., Reimold, U., and Koeberl, C. (2009) Isotopic
492 fractionation of zinc in tektites. *Earth and Planetary Science Letters*, 277, 482-489.
- 493 Moynier, F., Koeberl, C., Beck, P., Jourdan, F., and Telouk, P. (2010) Isotopic fractionation of
494 Cu in tektites. *Geochimica et Cosmochimica Acta*, 74, 799-807.
- 495 Mungall, J.E. (2002a) Kinetic controls on the partitioning of trace elements between silicate and
496 sulfide liquids. *Journal of Petrology*, 43, 749-768.
- 497 Mungall, J.E. (2002b) Empirical models relating viscosity and tracer diffusion in magmatic
498 silicate melts. *Geochimica et Cosmochimica Acta*, 66, 125-143.
- 499 Nadeau, O., Williams-Jones, A.E., and Stix, J. (2010) Sulphide magma as a source of metals in
500 arc-related magmatic hydrothermal ore fluids. *Nature Geoscience*, 3, 501-505.
- 501 Nadeau, O., Stix, J., and Williams-Jones, A.E. (2013) The behavior of Cu, Zn and Pb during
502 magmatic–hydrothermal activity at Merapi volcano, Indonesia. *Chemical Geology*, 342, 167-
503 179.
- 504 Naldrett, A.J. (1989) *Magmatic sulfide deposits*. Oxford University Press.
- 505 Ni, H., and Zhang, Y. (2008) H₂O diffusion models in rhyolitic melt with new high pressure
506 data. *Chemical Geology*, 250, 68-78.
- 507 Ni P., Zhang Y., Simon A. & Gagnon J. (2015) *Goldschmidt Abstracts*, 2015 2269.
- 508 Pearce, N.J., Perkins, W.T., Westgate, J.A., Gorton, M.P., Jackson, S.E., Neal, C.R., and
509 Chenery, S.P. (1997) A compilation of new and published major and trace element data for
510 NIST SRM 610 and NIST SRM 612 glass reference materials. *Geostandards newsletter*, 21,
511 115-144.
- 512 Ripley, E.M., and Brophy, J.G. (1995) Solubility of copper in a sulfur-free mafic
513 melt. *Geochimica et cosmochimica acta*, 59, 5027-5030.

- 514 Rudnick, R.L., and Gao, S. (2014) Composition of the continental crust, *Treatise on*
515 *Geochemistry* (2nd edition), pp. 1-51.
- 516 Shannon, R.T. (1976) Revised effective ionic radii and systematic studies of interatomic
517 distances in halides and chalcogenides. *Acta Crystallographica Section A: Crystal Physics,*
518 *Diffraction, Theoretical and General Crystallography*, 32, 751-767.
- 519 Simon, A.C., Pettke, T., Candela, P.A., Piccoli, P.M., and Heinrich, C.A. (2006) Copper
520 partitioning in a melt–vapor–brine–magnetite–pyrrhotite assemblage. *Geochimica et*
521 *Cosmochimica Acta*, 70, 5583-5600.
- 522 Singer, D.A. (1995) World class base and precious metal deposits; a quantitative
523 analysis. *Economic Geology*, 90, 88-104.
- 524 von der Gonna, G., and Russel, C. (2000) Diffusivity of various polyvalent elements in a
525 $\text{Na}_2\text{O} \cdot 2\text{SiO}_2$ glass melt. *Journal of non-crystalline solids*, 261, 204-210.
- 526 Walter, L.S. (1967) Tektite compositional trends and experimental vapor fractionation of
527 silicates. *Geochimica et Cosmochimica Acta*, 31, 2043-2063.
- 528 Wang, H., Xu, Z., Behrens, H., and Zhang, Y. (2009) Water diffusion in Mount Changbai
529 peralkaline rhyolitic melt. *Contributions to Mineralogy and Petrology*, 158, 471-484.
- 530 Williams, T.J., Candela, P.A., and Piccoli, P.M. (1995) The partitioning of copper between
531 silicate melts and two-phase aqueous fluids: an experimental investigation at 1 kbar, 800 C
532 and 0.5 kbar, 850 C. *Contributions to Mineralogy and Petrology*, 121, 388-399.
- 533 Zajacz, Z., Halter, W.E., Pettke, T., and Guillong, M. (2008) Determination of fluid/melt
534 partition coefficients by LA-ICPMS analysis of co-existing fluid and silicate melt inclusions:
535 controls on element partitioning. *Geochimica et Cosmochimica Acta*, 72, 2169-2197.

- 536 Zajacz, Z., and Halter, W. (2009) Copper transport by high temperature, sulfur-rich magmatic
537 vapor: Evidence from silicate melt and vapor inclusions in a basaltic andesite from the
538 Villarrica volcano (Chile). *Earth and Planetary Science Letters*, 282, 115-121.
- 539 Zhang, Y. (2008) *Geochemical Kinetics*. Princeton University Press.
- 540 Zhang, Y. (2010) Diffusion in minerals and melts: theoretical background. *Reviews in*
541 *Mineralogy and Geochemistry*, 72, 5-59.
- 542 Zhang, Y. (2015). Toward a quantitative model for the formation of gravitational magmatic
543 sulfide deposits. *Chemical Geology*, 391, 56-73.
- 544 Zhang, Y., and Ni, H. (2010) Diffusion of H, C, and O components in silicate melts. *Reviews in*
545 *Mineralogy and Geochemistry*, 72, 171-225.
- 546 Zhang, Y., Ni, H., and Chen, Y. (2010) Diffusion data in silicate melts. *Reviews in Mineralogy*
547 *and Geochemistry*, 72, 311-408.
- 548

549 **FIGURE 1.** Copper concentration profiles measured across the center sections of four synthesized
550 glass beads. Distances shown in the figure are relative to the approximate center of the glass
551 beads.

552

553 **FIGURE 2.** Illustration of the experimental design for our diffusion couple experiments (modified
554 from [Wang et al. 2009](#)). Interface between the two glass halves are aligned to be at the center of
555 the graphite heater to minimize temperature gradient. The scale in the figure is not exact.

556

557 **FIGURE 3.** Cu diffusion profile of experiment Cudiffcp 3.1. Probe results obtained on two
558 different days are in open symbols and closed symbols respectively. Traverses 3 to 5 were
559 moved down by 194 ppm to account for the background shift relative to traverses 1 and 2. The
560 diffusivity given in the figure is based on fit of all 5 traverses after the correction for the
561 background shift.

562

563 **FIGURE 4.** Optical microscope images of experimental charges. (a) Cudiffcp 3.1; (b) Cudiffcp
564 7.2. The Cu-free glass is on the top while the Cu-bearing glass is at the bottom. In (a), two pieces
565 of glasses were welded together after the experiment; position of the interface is indicated by the
566 two dents on both sides of the glasses. In (b), there is a large crack right at the interface after the
567 experiment. Red dashed lines show the position of microprobe traverses.

568

569 **FIGURE 5.** Cu concentration profiles for all diffusion couple experiments in this study. Different
570 symbols in each plot represent different traverses analyzed on the sample perpendicular to the
571 interface.

572 **FIGURE 6.** Arrhenius plot of all copper diffusion data obtained in this study. The linear fitting is
573 for 1 GPa experiments only. Errors shown on diffusivities are at 1σ level.

574

575 **FIGURE 7.** Comparison of Cu diffusivities obtained in this study to literature diffusivity data for
576 other elements in anhydrous basaltic melts unless otherwise indicated. a. Cu diffusivities at 0.5
577 GPa from this study; b. Cu diffusivities at 1.5 GPa from this study; c. Cu diffusivities at 1 GPa
578 from this study; d. Cu diffusivities in dry basaltic melt by Mungall's model ([Mungall 2002b](#)); e.
579 Cu diffusivities in $\text{Na}_2\text{Si}_2\text{O}_5$ melt at 1000-1400 °C and 1 bar ([von der Gonna and Russel 2000](#)); f.
580 S diffusivities at 1225-1450 °C and 0.5-1 GPa ([Freda et al. 2005](#)); g. H_2O_t diffusivities at 1 wt%
581 water, 400-1500 °C, and ≤ 1 GPa ([Zhang and Ni 2010](#)); h. Cl tracer diffusivities at 1250-1450 °C
582 and 0.5-1 GPa ([Alletti et al. 2007](#)); i. Li tracer diffusivities at 1300-1400 °C and 1 bar ([Lowry et](#)
583 [al. 1981](#)); j. Na tracer diffusivities at 1300-1400 °C and 1 bar ([Lowry et al. 1982](#)); k. Co tracer
584 diffusivities at 1300-1400 °C and 1 bar ([Lowry et al. 1982](#)); l. Zn diffusivities in anhydrous
585 rhyolite melt at 898-1400 °C and 0.01–1 GPa ([Baker and Watson 1988](#)).

586

587 **TABLE 1.** Chemical compositions of the synthesized basaltic glasses.

wt%	Et1		Et1Cu		Et2		Et2Cu	
	ave	sd (1 σ)	ave	sd (1 σ)	ave	sd (1 σ)	ave	sd (1 σ)
SiO ₂	47.26	0.39	46.18	0.72	46.92	0.51	47.27	0.46
TiO ₂	1.62	0.06	1.63	0.04	1.67	0.05	1.66	0.05
Al ₂ O ₃	17.52	0.27	18.17	0.64	17.72	0.85	17.21	0.40
FeO _t	10.47	0.21	10.67	0.14	10.58	0.20	10.73	0.25
MgO	5.83	0.07	5.84	0.10	5.89	0.13	5.88	0.08
CaO	10.69	0.06	10.69	0.06	10.51	0.08	10.58	0.05
Na ₂ O	4.45	0.12	4.45	0.08	4.40	0.11	4.43	0.08
K ₂ O	2.03	0.04	1.90	0.04	2.06	0.04	2.10	0.04
Cu (ppm)	122	35	1174	121	82	22	1193	93
Total	99.88		99.65		99.76		99.98	

588 Reported data are electron microprobe measurements of far-field compositions on the samples
589 after experiments, except for Cu, whose concentrations are measured on original glasses before
590 experiments. At least 20 points were analyzed and averaged for each glass composition. Details
591 about the microprobe analysis can be found in Analytical Methods.

592

593 **TABLE 2.** Summary of experimental conditions and results.

Exp#	<i>P</i> (GPa)	<i>T</i> (°C)	Duration (s)		<i>D</i> (10 ⁻¹² m ² /s)	Error (1σ)
			<i>t</i> ₁ (s)	<i>t</i> ₂ (s)		
Cudiffcp 1.1	1	1314	429.3	464.6	403.7*	37.1
Cudiffcp 1.2	1	1314	124.2	162.4	439.4	26.8
Cudiffcp 2.1	1	1397	126.4	162.7	678.3	43.7
Cudiffcp 3.1	1	1509	105.1	140.5	930.9	6.3
Cudiffcp 4.2	0.5	1313	122.1	157.2	505.8	55.9
Cudiffcp 4.3	0.5	1306	119.9	157.7	514.3	71.7
Cudiffcp 4.4	0.5	1298	131.2	161.8	355.3	31.9
Cudiffcp 5.1	1	1575	95.6	137.7	1237.3*	157.5
Cudiffcp 6.1	1.5	1410	125.7	151.1	465.5	28.9
Cudiffcp 7.2	1.5	1581	107.9	140.4	1104.6*	68.8

594 *P* is corrected pressure; *T* is corrected temperature; *t*₁ is the recorded duration at the target
 595 temperature ±1 °C; *t*₂ is the corrected duration using the method described in Experimental
 596 Procedure.
 597 *Diffusivities of these three experiments were fitted using the solution for a finite diffusion
 598 medium as explained in the text.

Fig. 1

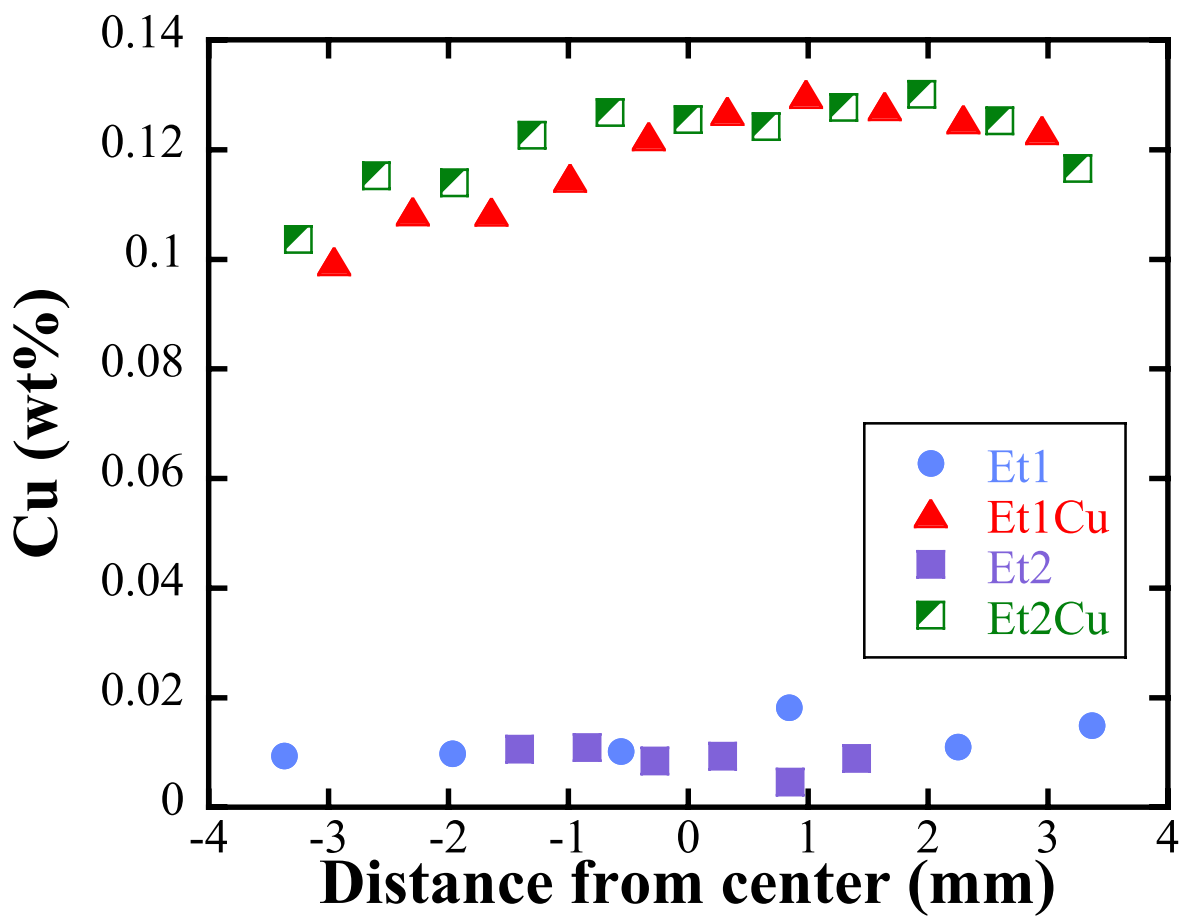


Figure 2

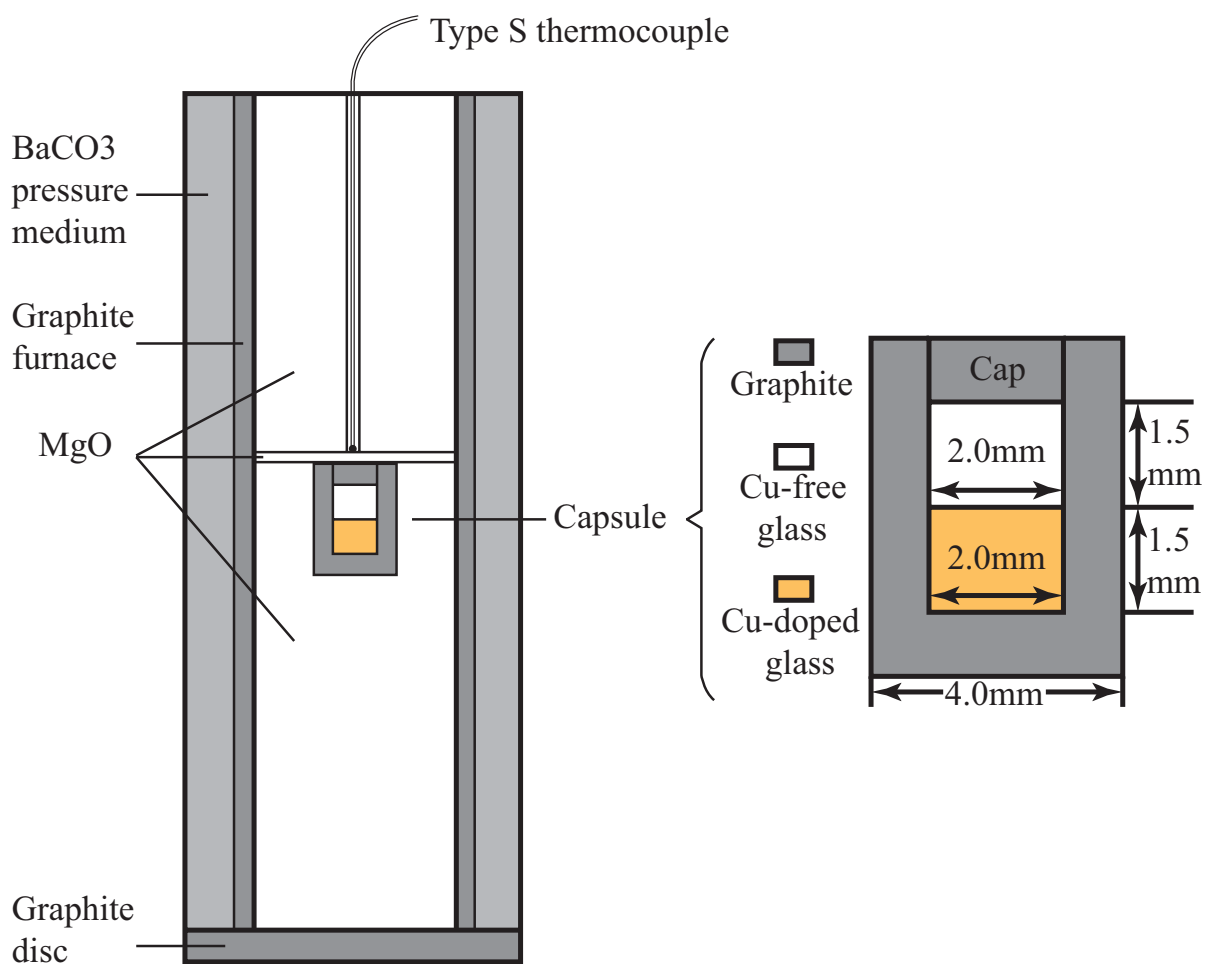


Fig. 3

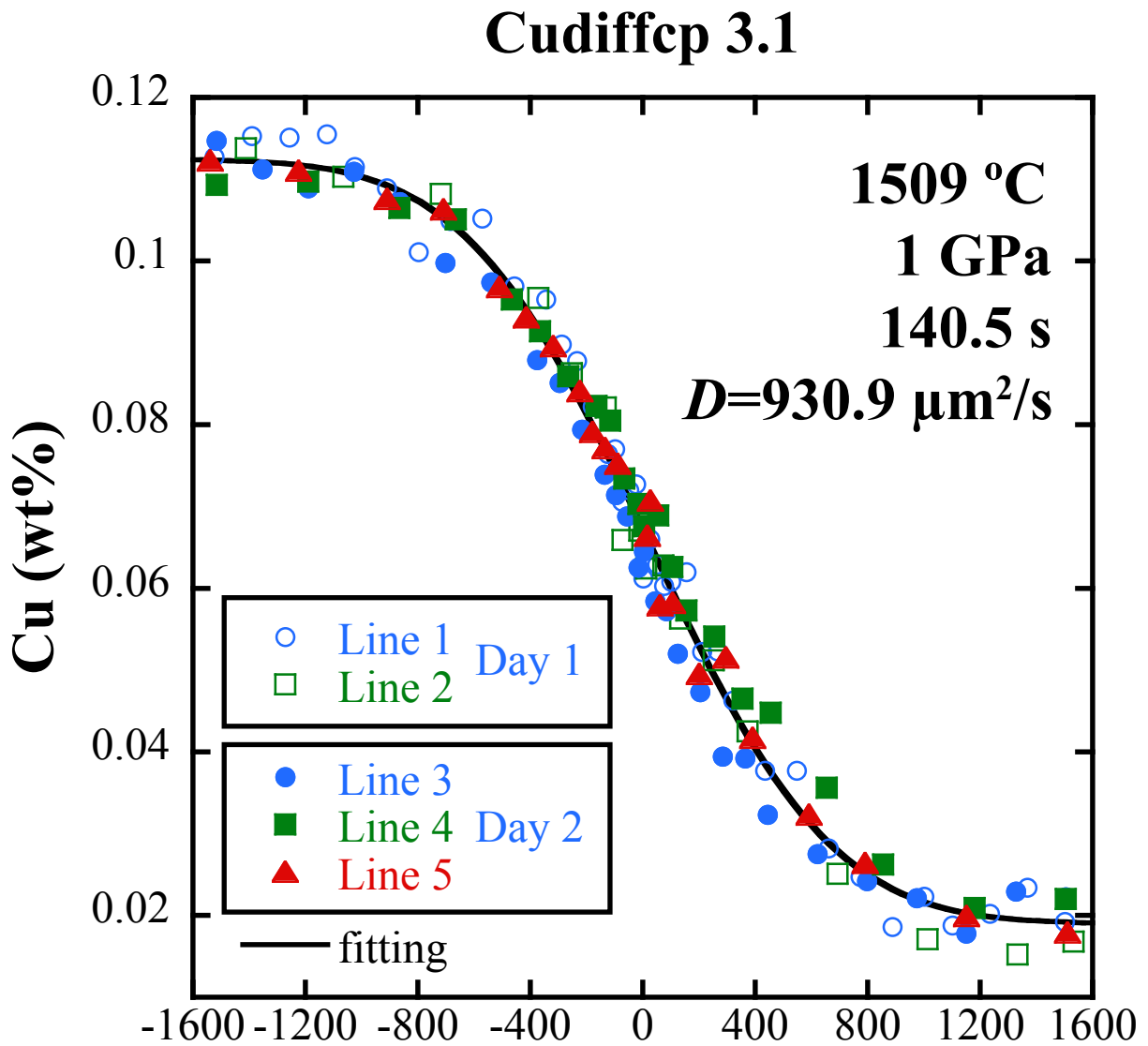


Fig. 4a

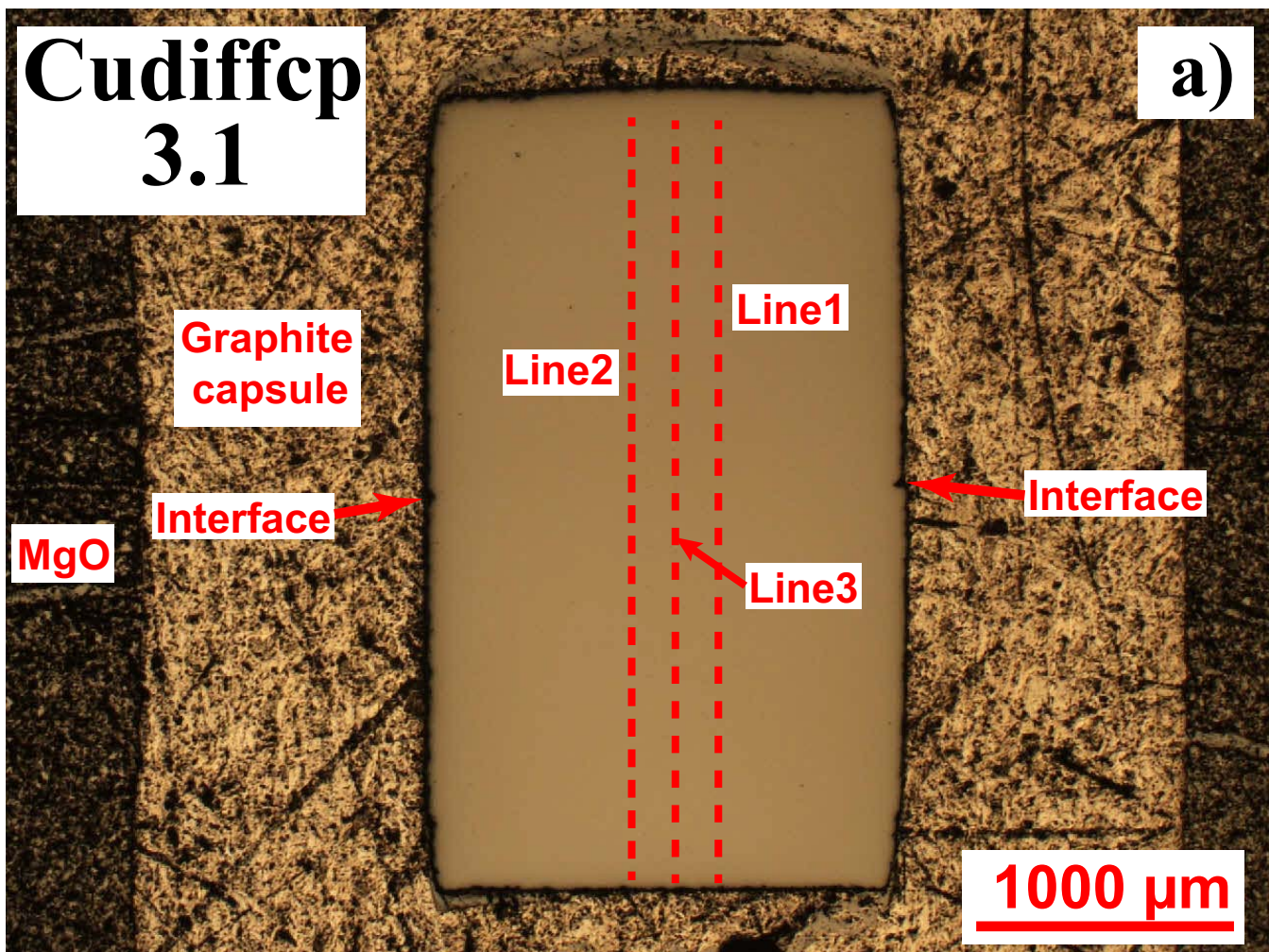


Fig. 4b

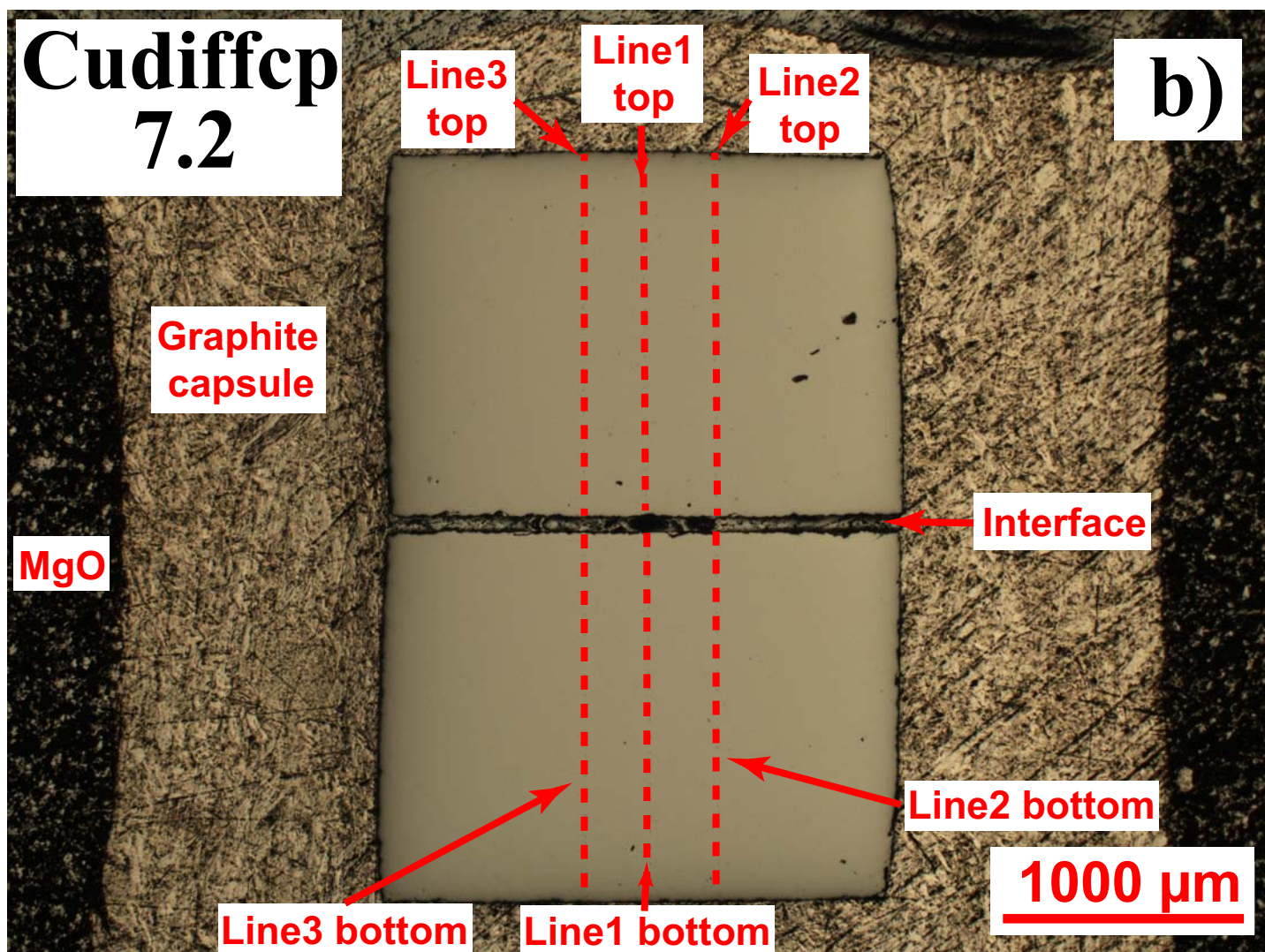


Fig. 5a

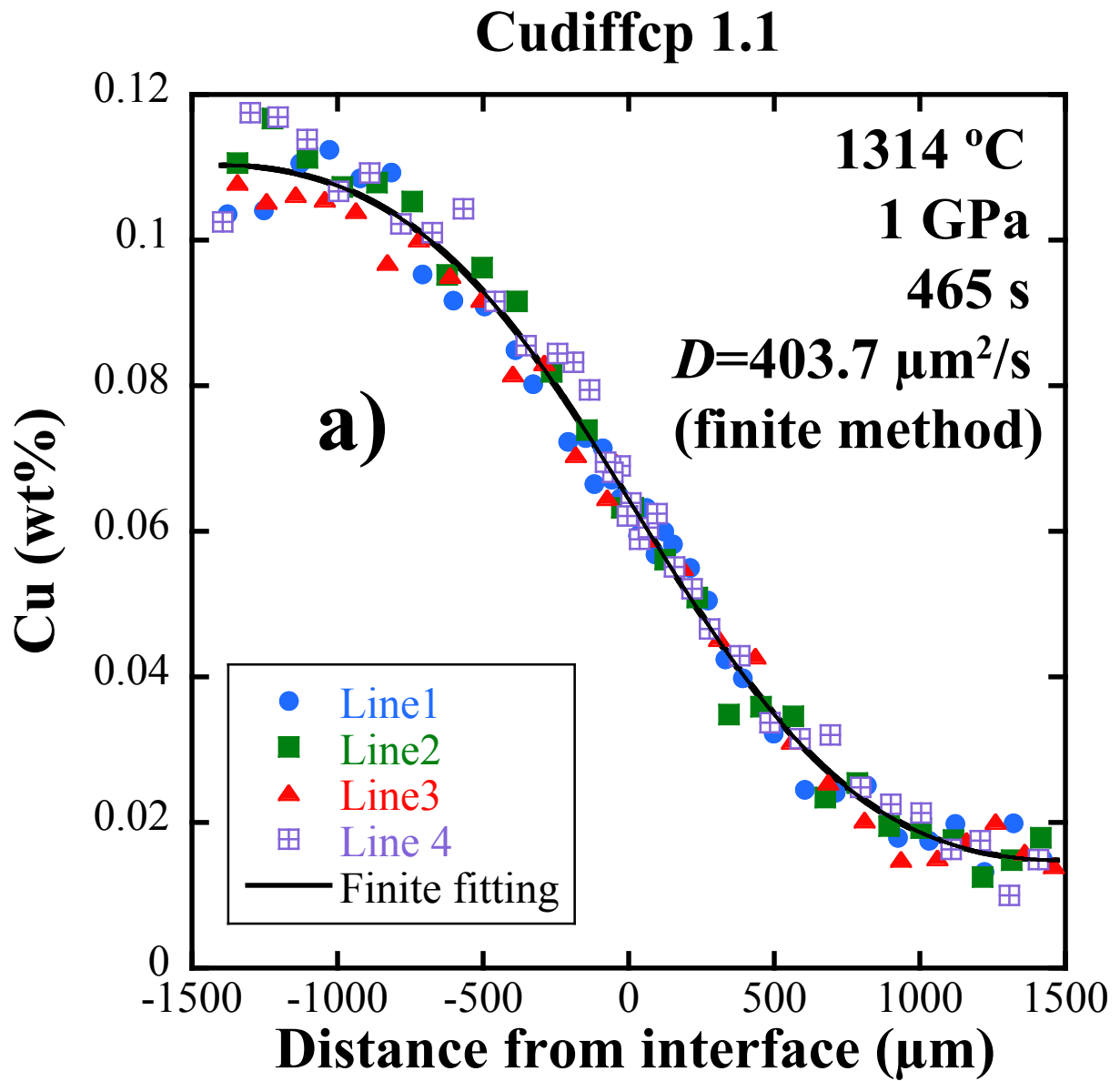


Fig. 5b

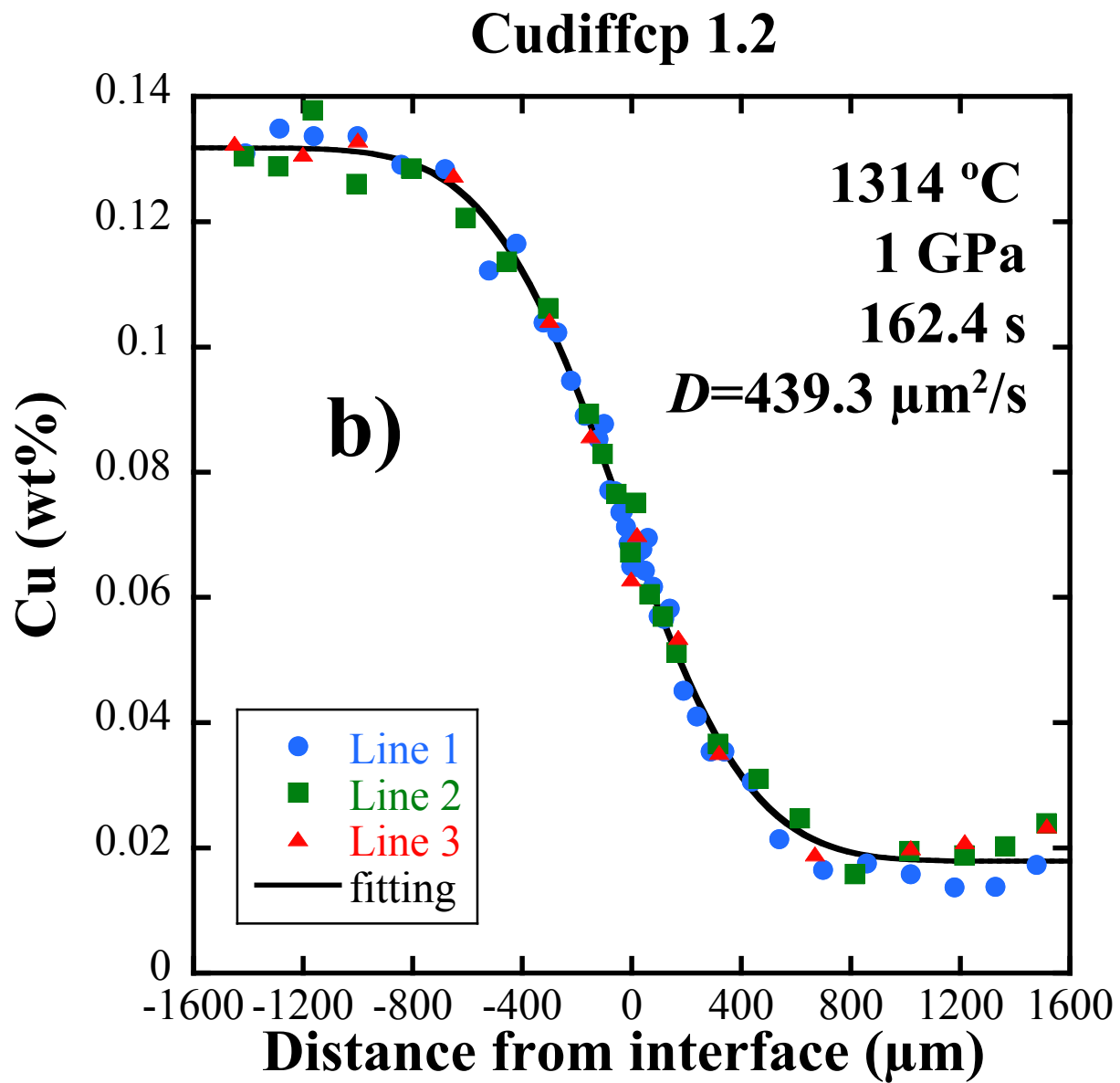


Fig. 5c

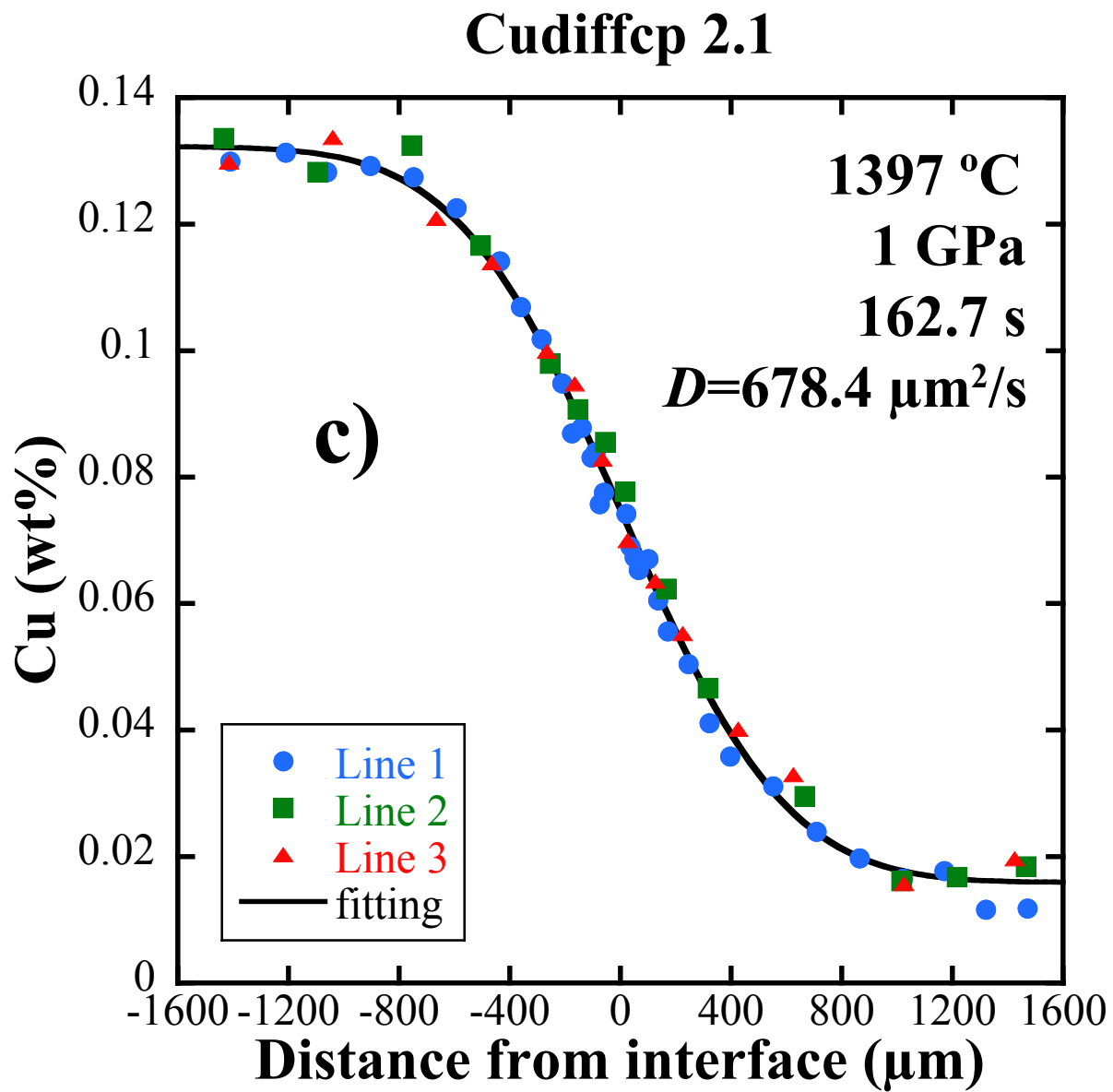


Fig. 5d

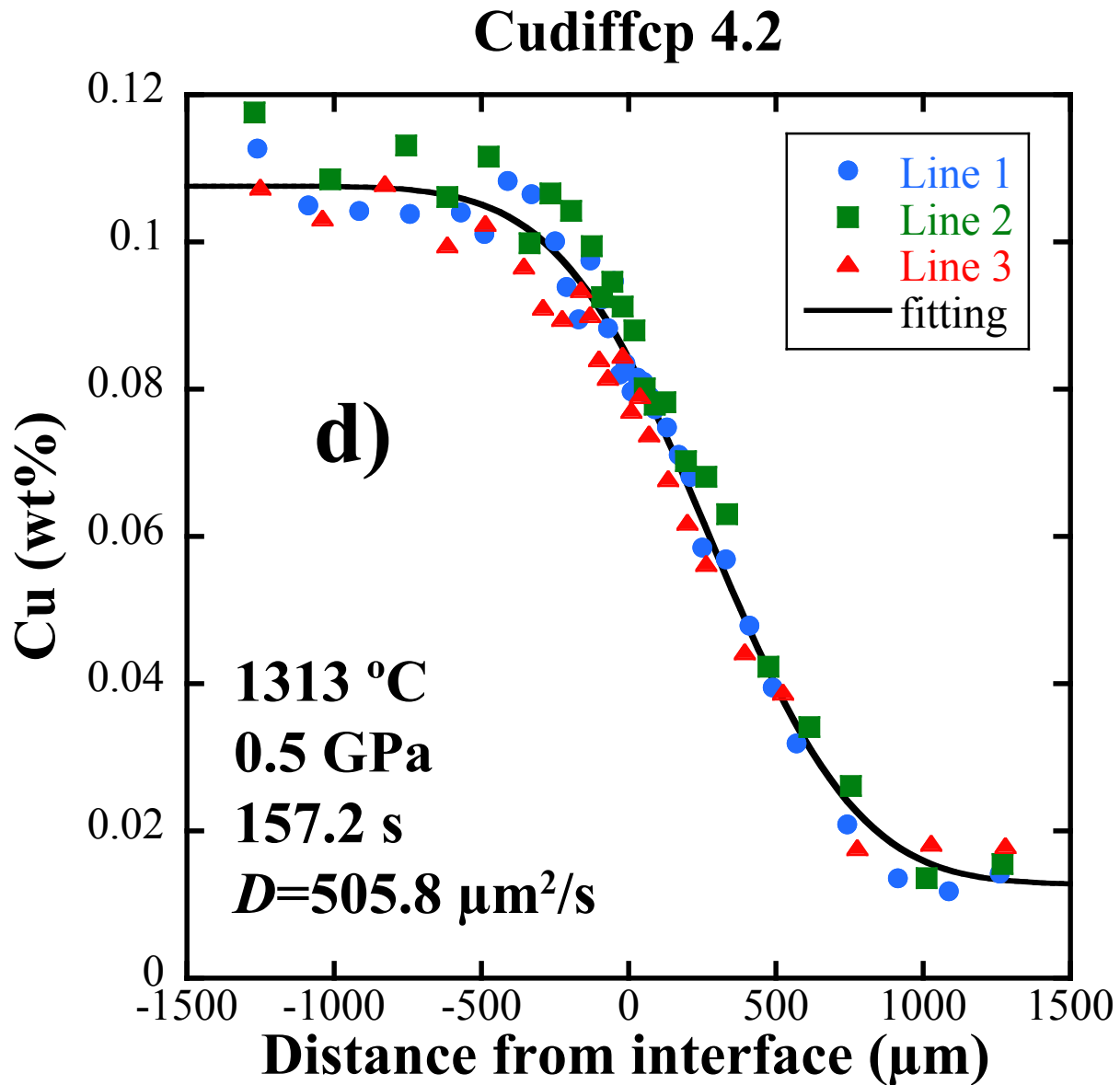


Fig. 5e

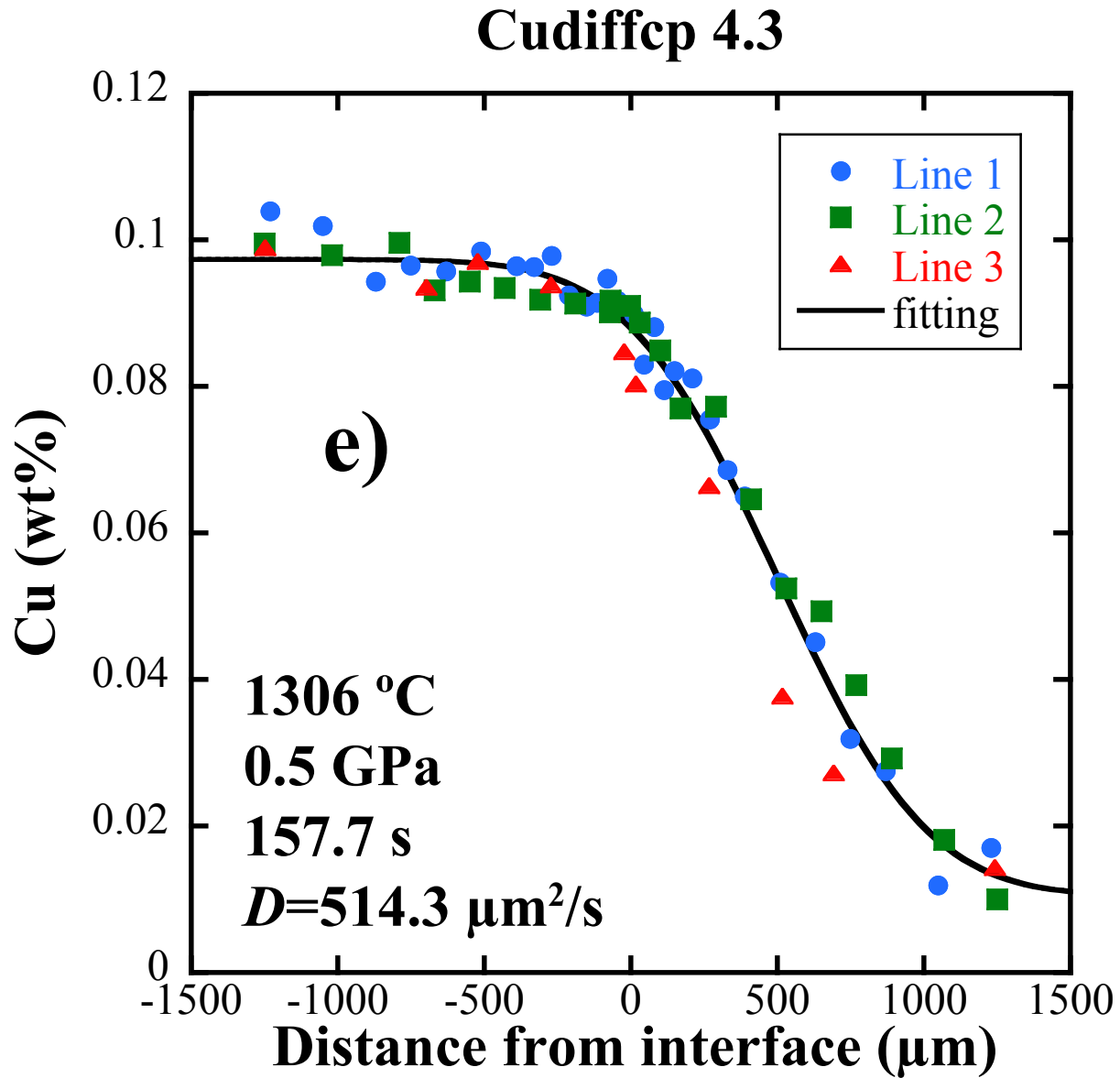


Fig. 5f

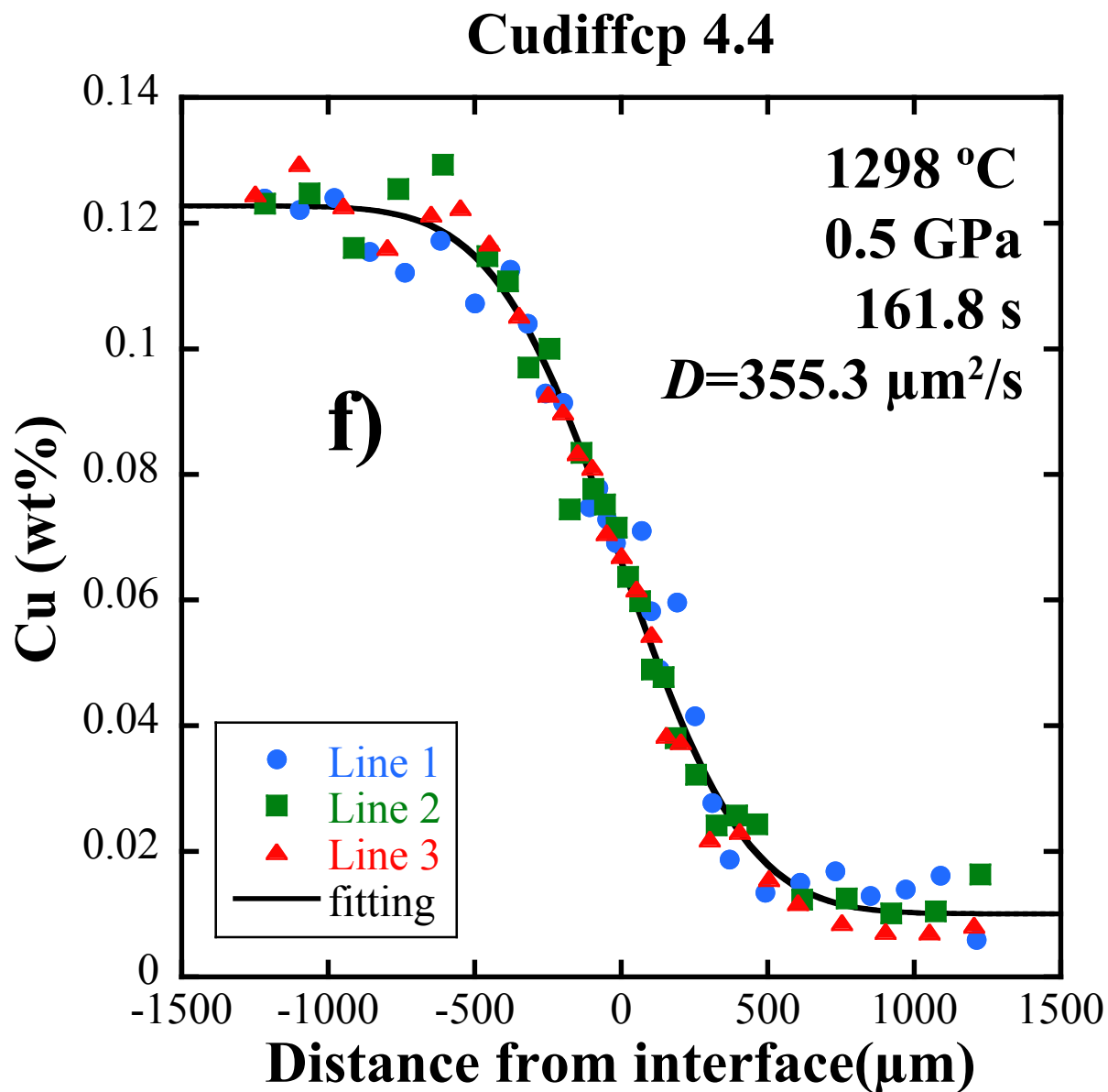


Fig. 5g

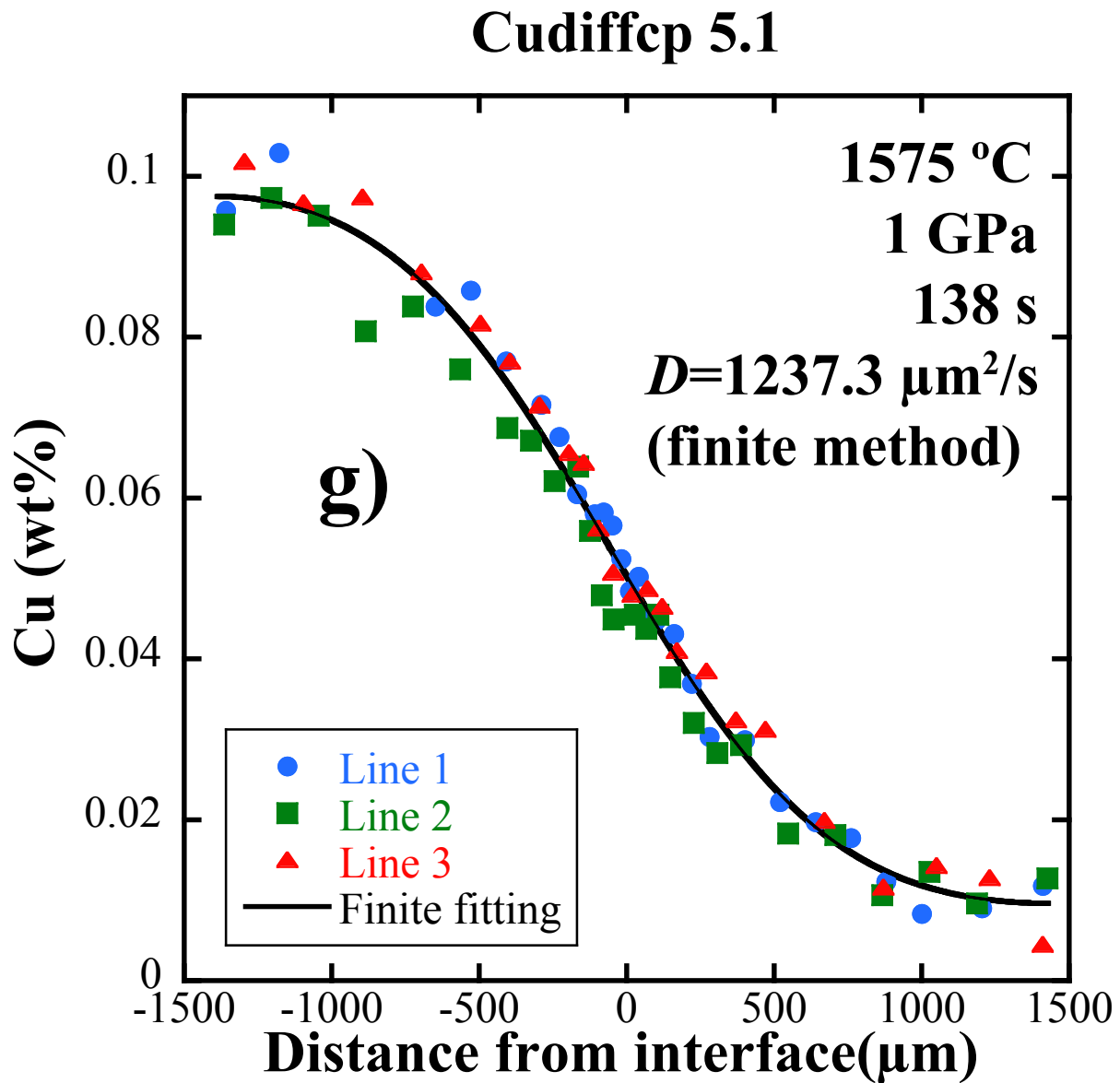


Fig. 5h

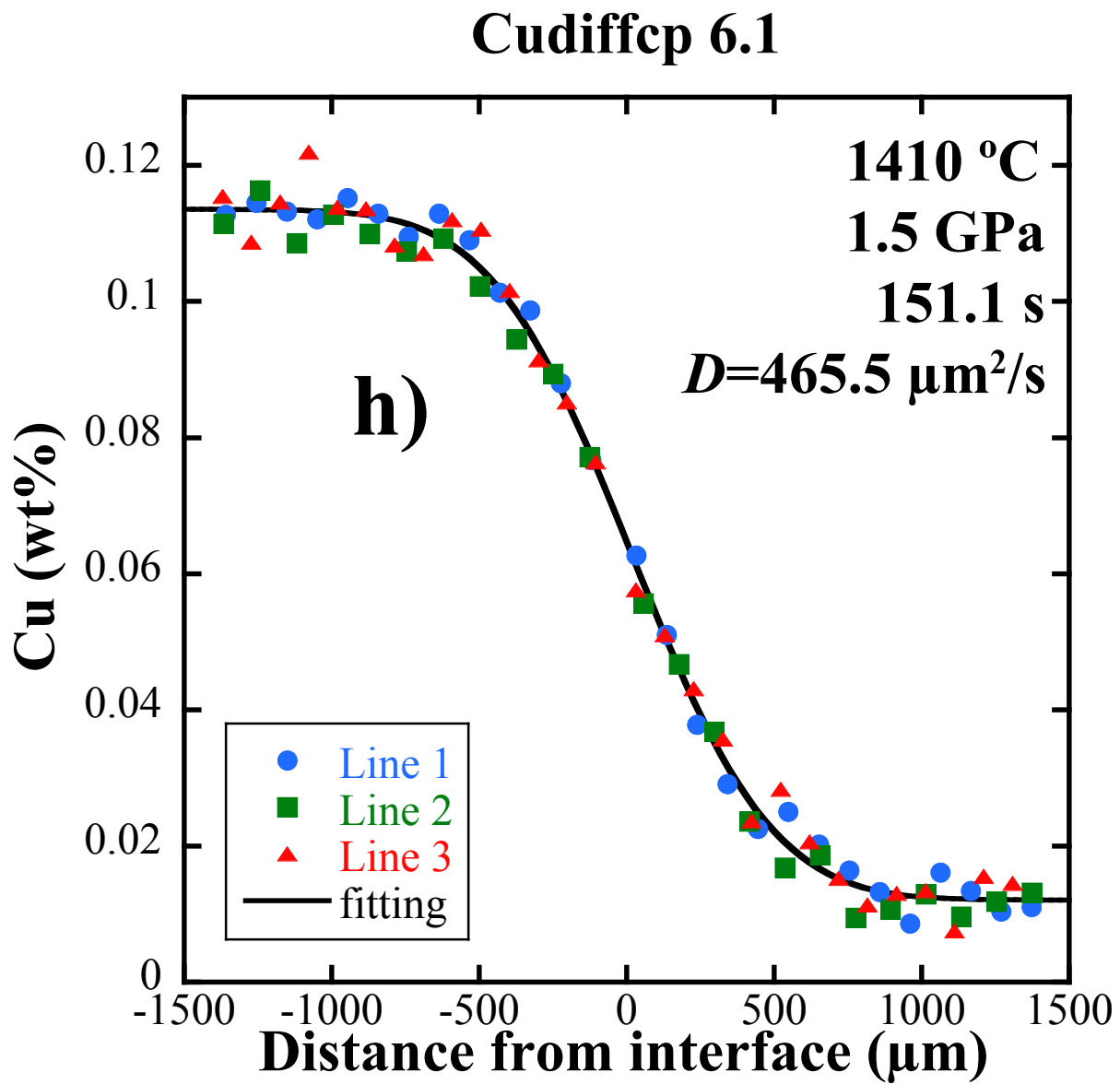


Fig. 5i

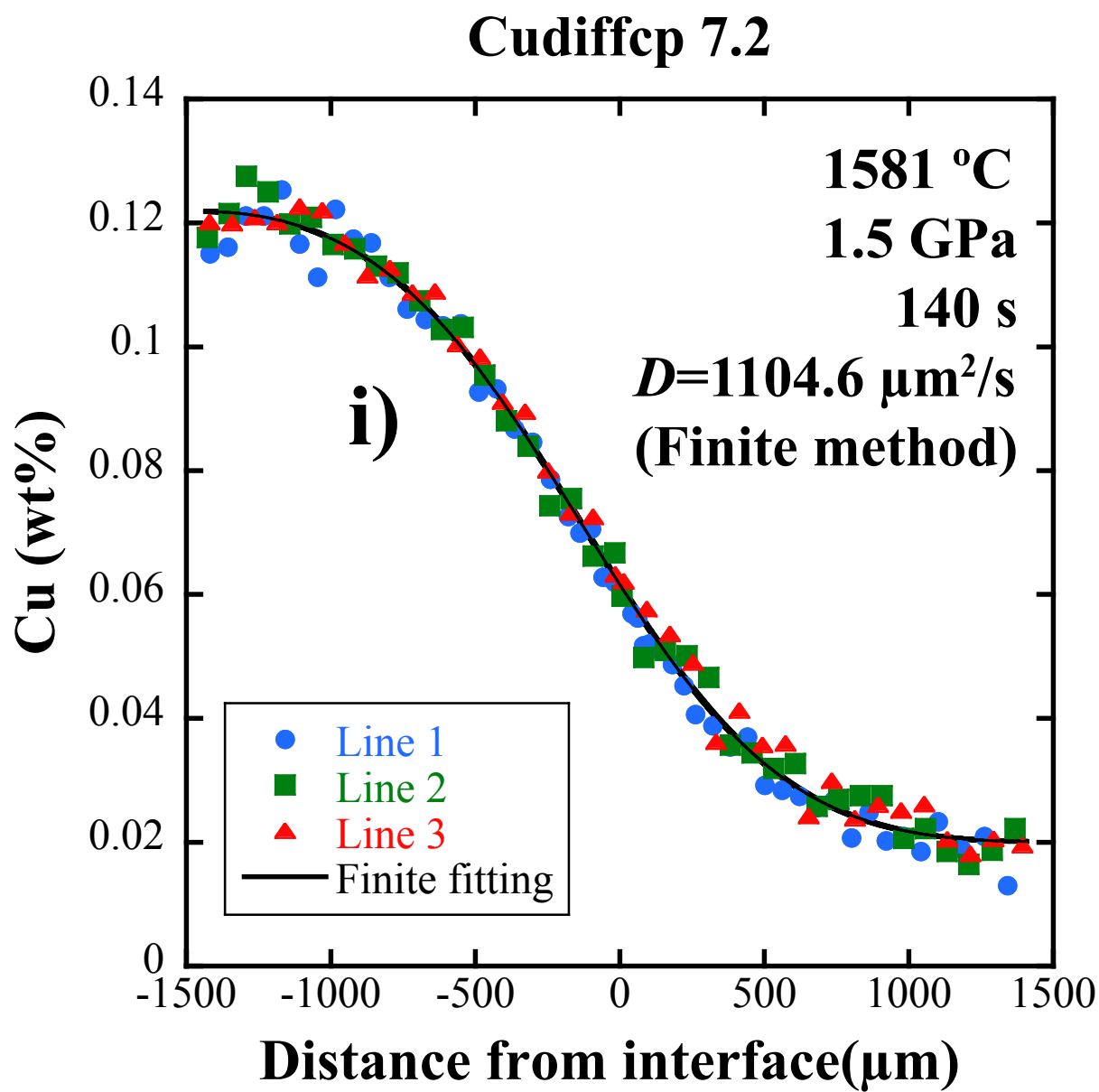


Fig. 6

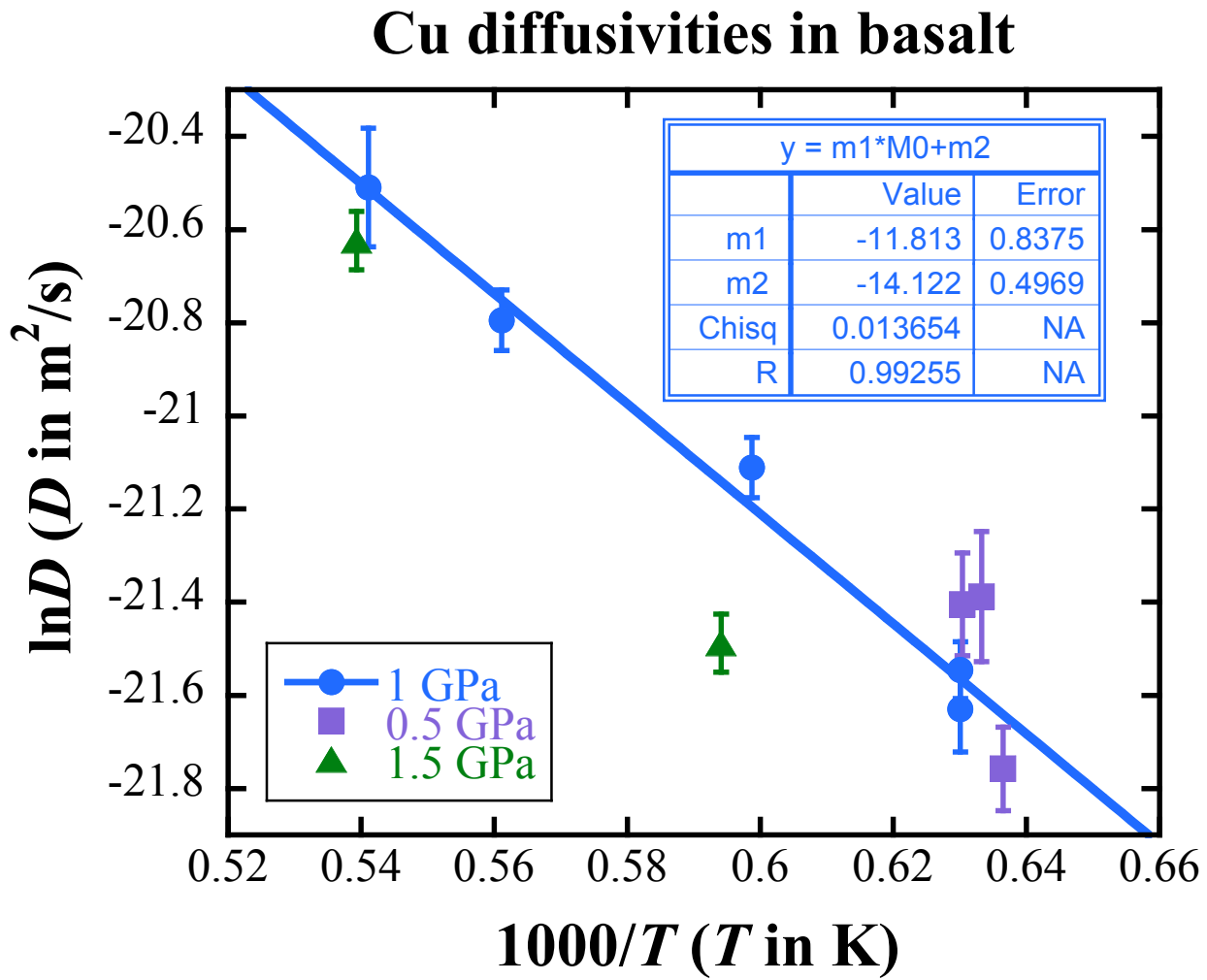


Fig. 7

